Earth and Planetary Science Letters 288 (2009) 255–267

Contents lists available at ScienceDirect

Earth and Planetary Science Letters

journal homepage: www.elsevier.com/locate/epsl

Iron isotopes may reveal the redox conditions of mantle melting from Archean to Present

Nicolas Dauphas [a,b,*], Paul R. Craddock [a], Paul D. Asimow [b], Vickie C. Bennett [c], Allen P. Nutman [d], Daniel Ohnenstetter [e]

[a] Origins Laboratory, Department of the Geophysical Sciences and Enrico Fermi Institute, The University of Chicago, 5734 South Ellis Avenue, Chicago, IL 60637, USA
[b] Division of Geological and Planetary Sciences, California Institute of Technology, Pasadena, CA 91125, USA
[c] Research School of Earth Sciences, The Australian National University, Canberra, ACT 0200, Australia
[d] Institute of Geology and Chinese International Centre for Precambrian Research, Chinese Academy of Geological Sciences, 26 Baiwanzhuang Road, Beijing, 100037, China
[e] Centre de Recherches Pétrographiques et Géochimiques, CNRS-Université de Nancy, 15 rue Notre-Dame-des-Pauvres, 54501 Vandoeuvre-lès-Nancy, France

ARTICLE INFO

Article history:
Received 3 June 2009
Received in revised form 14 September 2009
Accepted 16 September 2009
Available online 28 October 2009

Editor: R.W. Carlson

Keywords:
iron
isotope
redox
melting
mantle
island arc
Archean

ABSTRACT

High-precision Fe isotopic data for 104 samples, including modern and ancient (≥3.7 Ga) subduction-related magmas and mantle peridotites, are presented. These data demonstrate that mid-ocean ridge and oceanic-island basalts (MORBs and OIBs) have on average small, but distinctly (~+0.06‰) higher $^{56}Fe/^{54}Fe$ ratios than both modern and Eoarchean boninites and many island arc basalts (IABs) that are interpreted to form by large degrees of flux melting of depleted mantle sources. Additionally boninites and many IABs have iron isotopic compositions similar to chondrites, fertile mantle peridotites, Eoarchean mantle peridotites, and basalts from Mars and Vesta. The observed variations are best explained by the bulk silicate Earth having a near-chondritic iron isotopic composition, with ~+0.3‰ equilibrium isotope fractionation between Fe^{3+} and Fe^{2+} and preferential extraction of isotopically heavier, incompatible Fe^{3+} during mantle melting to form oceanic crust (as represented by MORBs and OIBs). A quantitative model that relates the iron isotopic composition of basaltic magmas to the degree of partial melting, Fe^{3+}/Fe^{2+} ratio, and buffering capacity of the mantle is presented. The concept that redox conditions may influence iron isotopic fractionation during melting provides a new approach for understanding the redox conditions of magma genesis on early Earth and Mars. Experimental and theoretical work is required to establish iron isotopic fractionation as an oxybarometer of mantle melting.

1. Introduction

Earth, Mars and Vesta experienced different redox conditions during planetary differentiation (e.g. Wadhwa, 2008). Following core formation, the silicate portions of all three bodies began at relatively low oxygen fugacity. Hydrogen loss (from reduction of H_2O) or production and subsequent removal of metal (from disproportionation of Fe^{2+} to Fe^0 and Fe^{3+}) drove the terrestrial mantle towards more oxidized conditions (e.g., Frost and McCammon, 2008). These processes may have left an imprint on the iron isotopic composition of Earth's crust.

The iron isotopic composition of the bulk silicate Earth (BSE) has been the subject of some controversy over the past several years (e.g., Weyer et al., 2005, 2007; Schoenberg and von Blanckenburg, 2006; Weyer and Ionov, 2007; Poitrasson, 2007; Beard and Johnson, 2007). Terrestrial basalts formed in a variety of tectonic settings have approximately homogeneous iron isotopic composition (Beard and Johnson, 1999; Beard et al., 2003; Poitrasson et al., 2004; Schoenberg and von Blanckenburg, 2006; Weyer and Ionov, 2007), which is enriched by ~+0.1 ‰ in $^{56}Fe/^{54}Fe$ ratio relative to chondrites (Poitrasson et al., 2004, 2005; Dauphas et al., 2004a; Schoenberg and von Blanckenburg, 2006). In contrast, basalts from Mars and Vesta have near-chondritic iron isotopic composition (Poitrasson et al., 2004; Weyer et al., 2005; Anand et al., 2006; Schoenberg and von Blanckenburg, 2006). Three interpretations have been proposed to explain the non-chondritic iron isotopic composition of MORBs, OIBs, and continental basalts. One is high-pressure (>100 GPa) equilibrium fractionation between metal and silicate during core formation (Polyakov, 2009), yielding a non-chondritic mantle that might be sampled by mid-ocean ridge magmatism. A second is kinetic isotope fractionation associated with evaporative loss of metallic iron during the Moon-forming impact (Poitrasson et al., 2004), again possibly yielding a non-chondritic mantle. Alternatively, the mantle source might be chondritic in its iron isotopic composition but the basalts derived from the mantle might be fractionated, e.g. if redox conditions influence how iron isotopes partition between liquid and solid during partial melting (Williams et al., 2005; Weyer and Ionov, 2007).

* Corresponding author. Origins Laboratory, Department of the Geophysical Sciences and Enrico Fermi Institute, The University of Chicago, 5734 South Ellis Avenue, Chicago, IL 60637, USA.
E-mail address: dauphas@uchicago.edu (N. Dauphas).

0012-821X/$ – see front matter © 2009 Elsevier B.V. All rights reserved.
doi:10.1016/j.epsl.2009.09.029

Table 1
Iron isotopic compositions of geostandards, chondrites, and terrestrial igneous rocks.

Sample type	Name/catalog no.	δ^{56}Fe (‰)	δ^{57}Fe (‰)
Geostandards and reference samples			
Granite, Ailsa Craig Island, Scotland	AC-E	0.309 ± 0.026	0.487 ± 0.039
Andesite, Oregon, USA	AGV-2	0.105 ± 0.017	0.152 ± 0.025
Basalt, Oregon, USA	BCR-2	0.087 ± 0.023	0.141 ± 0.040
Basalt, Hawaii, USA	BHVO-1	0.104 ± 0.014	0.162 ± 0.023
Dunite, Washington, USA	DTS-2B	0.017 ± 0.047	0.047 ± 0.043
Peridotite, California, USA	PCC-1	0.030 ± 0.021	0.059 ± 0.033
Pillow basalt, Hawaii, USA	T4D2#1	0.058 ± 0.032	0.104 ± 0.057
Chondrites			
Murchison (CM2)	MNHN no2435	−0.017 ± 0.020	−0.002 ± 0.030
Lancé (CO3)	Me 1351 #3	−0.017 ± 0.039	−0.036 ± 0.065
Allende (CV3)	USNM 3529	−0.004 ± 0.020	0.006 ± 0.028
Paragould (LL5)	Me 2135 #15	−0.029 ± 0.055	−0.053 ± 0.090
Saint-Séverin (LL6)	MNHN no2397	0.013 ± 0.039	0.015 ± 0.065
Farmington (L5)	Me 347 #10	−0.043 ± 0.032	−0.047 ± 0.045
Bielokrynitschie (H4)	Me 1394 #10	0.007 ± 0.037	−0.037 ± 0.058
Ochansk (H4)	Me 1443 #13	0.008 ± 0.055	−0.008 ± 0.090
Kernouvé (H6)	MNHN no602	0.017 ± 0.055	0.038 ± 0.090
Indarch (EH4)	Me 1404 #60	0.027 ± 0.029	0.033 ± 0.047
Saint-Sauveur (EH5)	MNHN no1456	−0.020 ± 0.033	0.007 ± 0.070
Blithfield (EL6 breccia)	Me 1979 #7	−0.140 ± 0.030	−0.191 ± 0.045
Hvittis (EL6 breccia)	Me 578 #4	0.032 ± 0.032	0.037 ± 0.045
Modern island arc basalts			
New Britain			
Basalt, New Britain	NMNH 116852-1	−0.037 ± 0.022	−0.043 ± 0.034
Basalt, New Britain	NMNH 116852-2	0.084 ± 0.031	0.119 ± 0.043
Basalt, New Britain	NMNH 116852-3	0.063 ± 0.032	0.112 ± 0.045
Basalt, New Britain	NMNH 116852-4	0.007 ± 0.029	−0.009 ± 0.043
Basalt, New Britain	NMNH 116852-5	0.039 ± 0.032	0.052 ± 0.045
Basalt, Unea	NMNH 116852-6	0.089 ± 0.023	0.154 ± 0.035
Basalt, Garove	NMNH 116852-7	0.124 ± 0.028	0.207 ± 0.051
Basalt, Garove	NMNH 116852-8	0.074 ± 0.029	0.107 ± 0.043
Basalt, Mundua	NMNH 116852-9	0.111 ± 0.028	0.145 ± 0.051
Basalt, Mundua	NMNH 116852-10	0.119 ± 0.032	0.185 ± 0.045
Basalt, Undaka	NMNH 116852-11	0.143 ± 0.022	0.228 ± 0.037
Basalt, Narage	NMNH 116852-12	0.054 ± 0.032	0.041 ± 0.045
Tonga			
Anorthite basalt, Eua	NMNH 111549-7	0.010 ± 0.032	−0.008 ± 0.045
Basaltic andesite, Hunga Ha'apai	NMNH 111550-1	0.049 ± 0.036	0.065 ± 0.069
Basaltic andesite, Hunga Ha'apai	NMNH 111550-3	0.033 ± 0.028	0.041 ± 0.044
Lava, Metis Shoal	NMNH 111108	0.050 ± 0.029	0.066 ± 0.043
Izu–Mariana			
Augite basalt, Agrihan	NMNH 108982-4	0.019 ± 0.029	0.043 ± 0.043
Augite basalt, Pagan	NMNH 108982-5	0.027 ± 0.029	0.028 ± 0.043
Augite basalt, Pagan	NMNH 108982-6	0.032 ± 0.028	0.034 ± 0.044
Augite basalt, Alamagan	NMNH 108982-7	0.068 ± 0.036	0.072 ± 0.069
Augite basalt, Pagan	NMNH 108982-8	0.025 ± 0.029	0.042 ± 0.043
Augite-hypersthene basalt, Saipan	NMNH 108982-37	0.119 ± 0.029	0.163 ± 0.054
Augite-hypersthene basalt, Saipan	NMNH 108982-107	0.101 ± 0.029	0.176 ± 0.054
Augite-hypersthene basalt, Saipan	NMNH 108982-135	0.083 ± 0.036	0.133 ± 0.069
Olivine basalt, O-shima	NMNH 112960	0.012 ± 0.029	−0.026 ± 0.042
Modern boninites			
Muko-Jima, Bonin islands	NMNH 116469	−0.010 ± 0.029	0.005 ± 0.054
Chichi-Jima, Bonin islands	780/67a	0.032 ± 0.032	0.045 ± 0.057
Chichi-Jima, Bonin islands	780/67c	0.023 ± 0.032	0.018 ± 0.057
Chichi-Jima, Bonin islands	780/67g	0.040 ± 0.031	0.076 ± 0.049
Chichi-Jima, Bonin islands	780/67h	0.024 ± 0.031	0.042 ± 0.049
Népoui, New Caledonia	BON 1	0.048 ± 0.031	0.115 ± 0.049
Népoui, New Caledonia	RB 1D	0.039 ± 0.033	0.075 ± 0.070
Népoui, New Caledonia	RB 2	0.032 ± 0.037	0.026 ± 0.058
Népoui, New Caledonia	RB 3	0.057 ± 0.037	0.126 ± 0.058
Népoui, New Caledonia	RB 5	0.012 ± 0.039	0.001 ± 0.065
Népoui, New Caledonia	RB 6	0.020 ± 0.033	0.012 ± 0.070
Népoui, New Caledonia	RB 7	0.033 ± 0.037	0.030 ± 0.058
Népoui, New Caledonia	RB 13	0.040 ± 0.037	0.047 ± 0.058
Népoui, New Caledonia	RB 14	0.016 ± 0.033	0.036 ± 0.070
Népoui, New Caledonia	RB 21	0.010 ± 0.037	0.046 ± 0.058
Népoui, New Caledonia	RBP 5	0.051 ± 0.039	0.053 ± 0.065
Népoui, New Caledonia	RBP 6	0.043 ± 0.033	0.042 ± 0.070
Népoui, New Caledonia	RPQ 1A	0.053 ± 0.039	0.049 ± 0.065
Népoui, New Caledonia	RB Pont7	0.016 ± 0.055	0.008 ± 0.090

Table 1 (*continued*)

Sample type	Name/catalog no.	δ^{56}Fe (‰)	δ^{57}Fe (‰)
Modern boninites			
Népoui, New Caledonia	RR 10	0.057 ± 0.039	0.071 ± 0.065
Népoui, New Caledonia	BON P	0.009 ± 0.055	0.049 ± 0.090
Eoarchean igneous rocks			
Amphibolites of IAB chemical affinity			
Isua 3.8 Ga basalt	G93-35	0.037 ± 0.032	0.072 ± 0.045
Isua 3.8 Ga basalt	JG03-40b	0.051 ± 0.029	0.077 ± 0.044
Isua 3.8 Ga basalt	JG03-42	0.050 ± 0.027	0.080 ± 0.042
Isua 3.8 Ga basalt	JG03-48	0.021 ± 0.028	0.024 ± 0.037
Isua 3.8 Ga basalt	JG03-52	0.038 ± 0.028	0.060 ± 0.037
Isua 3.8 Ga basalt	JG03-60	0.102 ± 0.032	0.143 ± 0.045
Isua 3.8 Ga basalt	JG03-62	0.014 ± 0.027	0.042 ± 0.042
Isua 3.8 Ga basalt	JG03-63	0.075 ± 0.017	0.108 ± 0.026
Isua 3.7 Ga amphibolite	G04-86	0.123 ± 0.038	0.198 ± 0.062
Isua 3.7 Ga amphibolite	G04-87	0.096 ± 0.029	0.151 ± 0.047
NW Isua 3.7 Ga amphibolite	G05-32	0.012 ± 0.027	0.004 ± 0.042
NW Isua 3.7 Ga amphibolite	G05-33	0.014 ± 0.027	−0.002 ± 0.042
Akilia >3.85 Ga metavolcanics	JG03-03	0.013 ± 0.029	0.020 ± 0.047
Akilia >3.85 Ga metavolcanics	G99-33	0.052 ± 0.021	0.069 ± 0.033
Amphibolites of boninite chemical affinity			
NE Isua 3.7 Ga boninite	G04-73A	0.032 ± 0.027	0.090 ± 0.042
NE Isua 3.7 Ga boninite	G04-73B	0.006 ± 0.028	0.000 ± 0.037
NE Isua 3.7 Ga boninite	G04-75	0.005 ± 0.028	0.023 ± 0.037
Mafic and ultramafic plutonic rocks			
S of Isua >3.8 Ga gabbros	G91-87	0.124 ± 0.038	0.218 ± 0.062
S of Isua >3.8 Ga gabbros	G97-22	−0.044 ± 0.025	−0.042 ± 0.046
S of Isua >3.8 Ga layered harzburgite	G93-72	0.163 ± 0.019	0.249 ± 0.028
SE Qilanngarssuit >3.85 Ga? gabbro	G91-30	0.045 ± 0.029	0.077 ± 0.047
SE Qilanngarssuit >3.85 Ga? gabbro	G93-149	0.060 ± 0.038	0.102 ± 0.062
SE Qilanngarssuit >3.85 Ga peridotite	G99-21	−0.054 ± 0.029	−0.068 ± 0.047
SE Qilanngarssuit >3.85 Ga? peridotite	G01-54	−0.030 ± 0.038	−0.034 ± 0.062
SE Qilanngarssuit >3.85 Ga? peridotite	G01-56	−0.038 ± 0.038	−0.035 ± 0.062
SE Qilanngarssuit >3.85 Ga? peridotite	G01-84	0.026 ± 0.029	0.054 ± 0.044
Tonalites			
S of Isua 3.8 Ga tonalite	G97-18	0.146 ± 0.027	0.186 ± 0.042
W of Akilia 3.85 Ga tonalite	G01-113	0.070 ± 0.026	0.119 ± 0.039
Qilanngarssuit 3.85 Ga tonalite	G99-22	0.011 ± 0.028	0.022 ± 0.037
N of Isua 3.70 Ga tonalite	3.7	0.139 ± 0.028	0.210 ± 0.037
Peridotites of probable mantle origin			
S of Isua >3.8 Ga dunite	G93-42	0.013 ± 0.020	0.016 ± 0.029
S of Isua >3.8 Ga dunite	G93-48	0.128 ± 0.028	0.191 ± 0.043
NW Isua ~3.7 Ga dunite	G05-35	0.019 ± 0.015	0.012 ± 0.024
NW Isua ~3.7 Ga dunite	G07-09	0.012 ± 0.029	0.037 ± 0.047
NW Isua ~3.7 Ga dunite	G07-10	0.036 ± 0.027	0.011 ± 0.042
NW Isua ~3.7 Ga dunite	G07-35	0.019 ± 0.027	0.028 ± 0.042
SE Narssaq >3.82 Ga dunite	G01-03	−0.070 ± 0.022	−0.106 ± 0.032
SE Narssaq >3.82 Ga dunite	G01-05	0.016 ± 0.019	0.025 ± 0.029

Error bars are 95% confidence intervals. A complete data table including replicate iron isotope analyses and major element compositions is available in Appendix A.

Important data that bear on the issue of the composition of the silicate Earth are the measurements of mantle peridotites by Weyer and Ionov (2007). In these samples, the iron isotopic composition $\{\delta^{56}Fe = [(^{56}Fe/^{54}Fe)_{sample}/(^{56}Fe/^{54}Fe)_{IRMM\text{-}014} - 1] \times 1000$, where IRMM-014 is a reference material with near-chondritic $^{56}Fe/^{54}Fe$ ratio} and degree of melt extraction $\{Mg\# = Mg/(Mg + Fe)_{molar}\}$ appear to be correlated. The slope of the correlation is consistent with ~+0.1‰ fractionation between melt and solid. The δ^{56}Fe value of the fertile mantle inferred from this correlation is ~+0.02 to +0.05‰, suggesting a near-chondritic value for the fertile upper-mantle. If Earth's mantle had a near-chondritic iron isotopic composition, then what is the mechanism responsible for the iron isotopic fractionation between Earth's crust and mantle? How is it influenced by degree of melting and iron oxidation state? Has this fractionation changed over geological time?

Previous high-precision studies of basalts have focused on Phanerozoic (<542 Ma) MORBs and OIBs formed by decompression melting (Poitrasson et al., 2004; Schoenberg and von Blanckenburg, 2006; Weyer and Ionov, 2007; Teng et al., 2008; Schuessler et al., 2009). Some subduction-related magmatic rocks have been studied and these have δ^{56}Fe values comparable to or heavier than MORBs and OIBs (Heimann et al., 2008 and references therein). However, only a few of these samples were from intra-oceanic subduction systems. To more fully examine the processes that cause iron isotopic fractionation during mantle melting, we have analyzed a set of well-characterized Eoarchean and Phanerozoic igneous rocks (Table 1) formed by flux melting (i.e. lowering of the solidus by influx of volatiles) of variably depleted mantle sources (boninites and island arc basalts—IABs). All Eoarchean samples (>3.6 Ga) are from the Itsaq Gneiss Complex of southern West Greenland (Nutman et al., 1996) and are from amphibolite units demonstrated to be of IAB and boninite affinity from their bulk chemistry (Polat et al., 2002; Polat and Hofmann, 2003; Jenner et al, 2009). Modern (Phanerozoic) IABs are from New Britain, Tonga, and Izu–Mariana intra-oceanic arc systems (BVSP, 1981). Modern boninites are from New Caledonia and Bonin Islands and are classified as types 1 and 3 low-Ca boninites, representing high degree partial melts of very depleted mantle sources (Crawford et al., 1989).

2. Materials and methods

2.1. Analytical methods

Dauphas et al. (2004a, 2009) have described the method used for iron isotopic analyses at the University of Chicago and the reader is referred to these contributions for details. Samples were carefully selected to avoid alteration. Most rock samples were rinsed with milli-Q water and acetone and rock fragments were powdered in an agate mortar. For Eoarchean rocks processed at the Australian National University, samples were hand chipped into small fragments, and powders prepared from interior pieces in an Al_2O_3 mill. For all samples, powder aliquots of ~5—20 mg were transferred to Teflon vials for digestion. Most samples were readily digested in vials with standard mixtures of HF–HNO_3–$HClO_4$ and HCl–HNO_3–$HClO_4$. Aluminous spinels or chromites in Eoarchean peridotites could not be dissolved in regular vials. These phases were digested at ~180 °C in Parr bombs using HF–HNO_3. After dissolution, iron was separated from matrix elements and potential isobars by anion-exchange chromatography in HCl medium (Strelow, 1980). At high HCl molarity (6 M), Fe was efficiently retained by AG1-X8 resin while other elements passed through the column. Iron was then eluted with HCl at lower molarity (0.4 M). Purified Fe was analyzed by multi-collector inductively coupled plasma mass spectrometry (MC-ICPMS). Instrumental mass fractionation was corrected for by standard bracketing with IRMM-014 reference material (Taylor et al., 1992). The measurements were carried out in medium and high mass resolution modes to resolve argide interferences from Fe isotopes (Malinovsky et al., 2003; Weyer and Schwieters, 2003; Arnold et al., 2004; Poitrasson and Freydier, 2005; Schoenberg and von Blanckenburg, 2005). Quoted precisions of ~±0.03‰ (95% confidence interval) on δ^{56}Fe take into account the stability of the bracketing standard measured during the analytical session as well as the long term external reproducibility of geostandard BHVO-1. Dauphas et al. (2009) demonstrated that the Fe isotopic analyses are accurate at this level of precision. Additional tests of accuracy directly relevant to this study are presented below (Fig. 1, Appendix A).

Iron isotopic analyzes can potentially be compromised by interferences of $^{54}Cr^+$, $^{40}Ar^{14}N^+$, $^{40}Ar^{16}O^+$, and $^{40}Ar^{16}O^1H^+$ on $^{54}Fe^+$, $^{56}Fe^+$, and $^{57}Fe^+$. The interference of $^{54}Cr^+$ was monitored and corrected for by analyzing $^{53}Cr^+$. Argide interferences were resolved from Fe isotopes using medium and high mass resolution. If any interference remained, this would have moved the data points away from the mass fractionation line. Despite the narrow range of δ^{56}Fe variations, all data

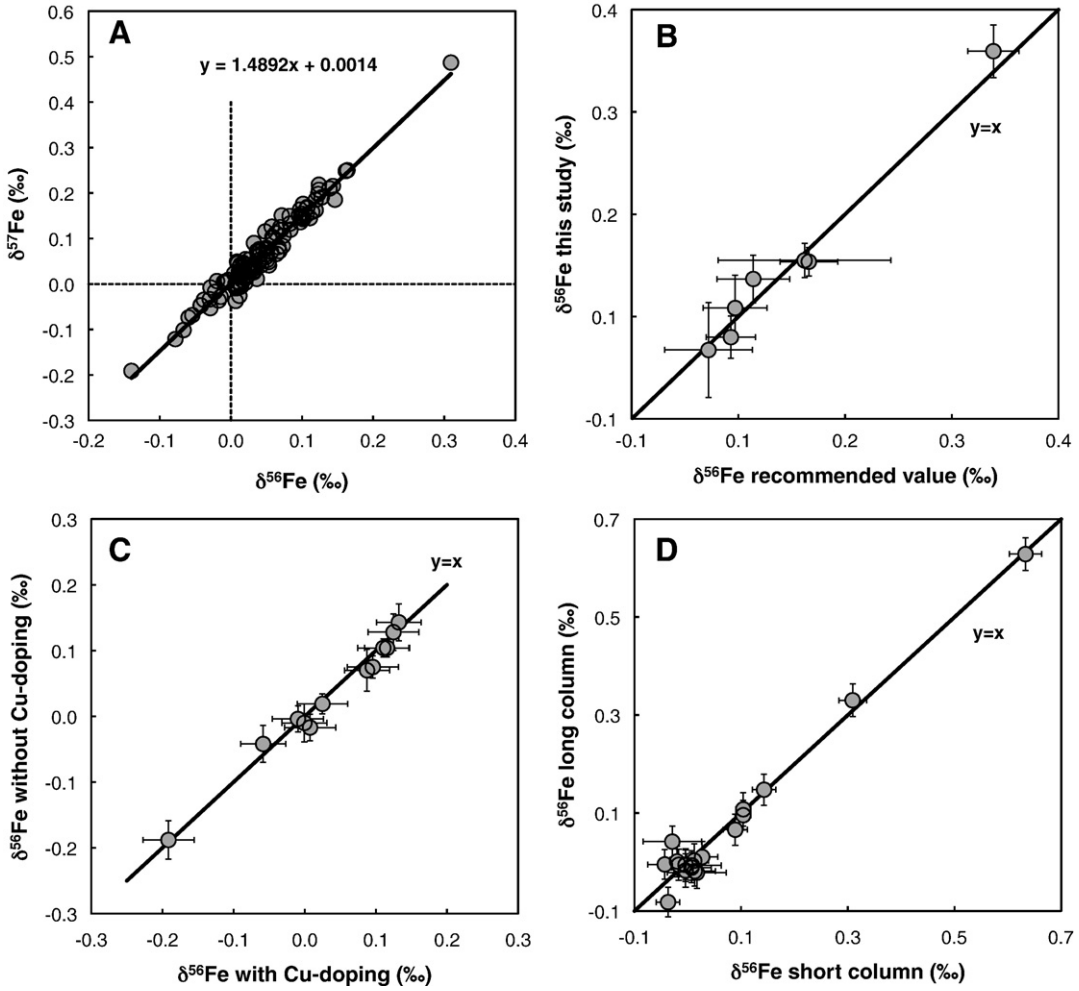

Fig. 1. Evaluation of the accuracy of iron isotopic analyses (data in Appendix A). A. Mass fractionation in δ^{56}Fe–δ^{57}Fe space. The data points define a straight line that goes through the origin and has a slope of ~(57–54)/(56–54) = 1.5, in agreement with theoretical expectation and previously documented mass fractionation law in natural materials (e.g. Malinovsky et al. 2003). B. Comparison between recommended δ^{56}Fe values of geostandards and reference samples (*x*-axis, Dauphas and Rouxel 2006; Teng et al. 2008) and results obtained in this study (*y*-axis). C. Comparison between Fe isotopic compositions measured by standard bracketing with (*x*-axis) and without (*y*-axis) Cu-doping. D. Comparison between Fe isotopic compositions measured with the protocol described by Dauphas et al. (2009)—short column) with one that is more time-consuming but improves separation of Fe from Cu (Tang et al., 2009—long column). Error bars represent 95% confidence intervals.

points follow very closely mass-dependent fractionation (Fig. 1A), demonstrating that the measurements are free of isobaric interferences.

The isotopic compositions of several geostandards and reference samples were measured repeatedly (AC-E granite, AGV-2 andesite, BCR-2 basalt, BHVO-1 basalt, DTS-2B dunite, PCC-1 peridotite, T4D2#1 basalt). These rocks were selected because they have matrices similar to the samples measured in this study and their δ^{56}Fe values are known from previous work. There is excellent agreement between δ^{56}Fe values reported here and recommended compositions (Fig. 1B; Dauphas and Rouxel, 2006; Teng et al., 2008).

If matrix elements were not eliminated by anion-exchange chromatography, this could affect instrumental mass fractionation and cause inaccuracy. Another way of correcting instrumental fractionation is to dope the solutions with Cu and assume that instrumental mass bias is identical for Cu and Fe. While this is not strictly true, it represents a good diagnostic tool to recognize the presence of matrix effects. Indeed, if such effects were present, δ^{56}Fe measured by standard bracketing alone and standard bracketing plus Cu-doping would be different (unless Cu is insensitive to matrix effects, which is unlikely). We measured several samples by standard bracketing with and without Cu-doping and there is excellent agreement between the two data sets (Fig. 1C). This is true for 3 basalts from New Britain island arc (116852-1, 6, 11) that span the whole range of δ^{56}Fe values measured at that location.

While the method for routine purification of Fe described by Dauphas et al. (2009) is very efficient, we have recently developed a modified procedure aimed at measuring departure from mass fractionation law at high precision (Tang et al., 2009). The aspect ratio of the column was modified (from a length of 2.0 cm to 10.5 cm) in order to increase the number of theoretical plates (Martin and Synge, 1941) and an elution step with 4 M HCl was introduced before elution of Fe to eliminate Cu (Strelow, 1980). The column separation procedure was repeated 2 to 3 times. We measured a suite of samples using this method. If chemical separation fractionated Fe isotopes because of incomplete recovery or if matrix elements eluted together with Fe affected instrumental mass bias, the results obtained with both procedures would likely differ. As shown in Fig. 1D, there is excellent agreement between the two methods. Again, this has been verified for 3 basalts from New Britain island arc (116852-1, 6, 11) that span the whole range of δ^{56}Fe values measured at that location.

2.2. Sample descriptions

2.2.1. Chondrites

A total of 13 chondrites were analyzed (Allende, Murchison, Hvittis, Farmington, Indarch, Blithfield, Bielokrynitschie, Saint-Sauveur, Lancé, Saint-Séverin, Ochansk, Paragould, Kernouvé). They represent 8 major chondrite classes (CM, CO, CV, L, LL, H, EH, EL), and cover most of the range of iron content and oxidation state found in undifferentiated meteorites (e.g. Sears and Dodd, 1988). Brecciated EL6 chondrite Blithfield shows evidence for extensive iron remobilization (Rubin, 1984).

2.2.2. Modern island arc basalts (IABs)

Three modern intra-oceanic-island arcs from the SW Pacific were studied. Focus is given below to New Britain as more basalts from this arc were analyzed.

2.2.2.1. New Britain. All 12 samples in the *Island Arc Basalt Reference Suite* of BVSP (1981) were analyzed. These samples were provided by the Smithsonian Institution (catalog nos. NMNH 116852-1 to 116852-12) and have been extensively characterized for their chemical and radiogenic isotope compositions (e.g. BVSP, 1981; Woodhead and Johnson, 1993; Woodhead et al., 1998). Quaternary volcanoes (<1.8 Ma) of the New Britain arc in Papua New Guinea formed as a result of the northward subduction of the Solomon plate beneath the Bismarck plate at a convergence rate of ~10 cm/yr. The present configuration of subduction and plate kinematics was established recently, following plate reorganization that was triggered by collision of the Ontong–Java Plateau with the Manus–Kilinailau trench at about 10 Ma (e.g. Petterson et al., 1999; Mann and Taira, 2004). The New Britain Arc is unique in that Quaternary volcanism extends over large distances away from the trench (Fig. 2A) corresponding to depths to the Wadati–Benioff zone from 100 km at the volcanic front to 600 km beneath the Witu Islands. Johnson (1977) divided the volcanoes into 6 zones parallel to the trench (E, F, Gs, Gn, Hs, and Hn) that overlie progressively deeper parts of the subducting slab. The samples span a narrow range of chemical compositions, from 49.2 to 53.1 wt.% SiO_2. Major and trace element characteristics show similarities with other "fluid-dominated" arcs (e.g. enrichment in LILEs relative to HFSEs, high Ba/La). Isotopic studies (e.g. ^{10}Be, Pb, Hf) indicate that the recycled component involved in the generation of the lavas is dominated by altered oceanic crust rather than sediment (Morris et al., 1990; Woodhead and Johnson, 1993; Woodhead et al., 2001). U-series data also constrain the residence time of slab-derived U in the mantle wedge prior to magma genesis to more than 10^5 yr (Gill et al., 1993). Lavas from the New Britain Island Arc are extremely depleted in HFSEs. An interpretation put forward by Woodhead et al. (1998) is that this

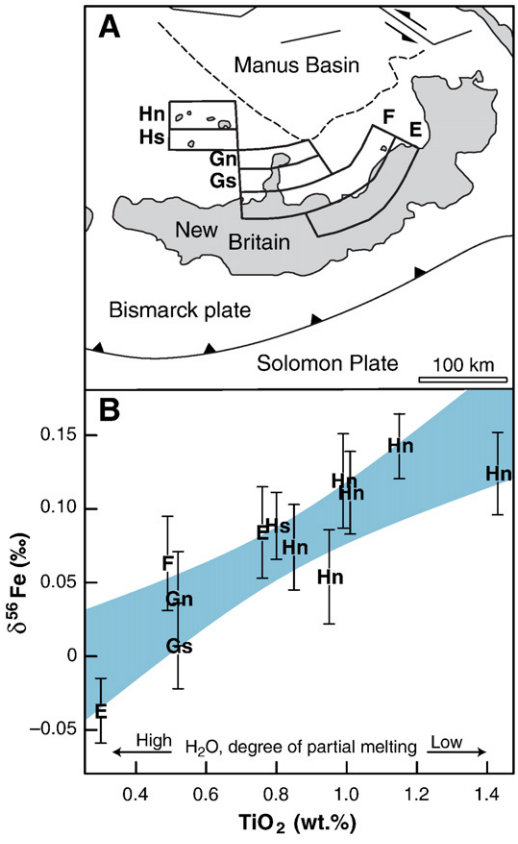

Fig. 2. Tectonic setting and iron isotopic compositions of island arc basalts (IABs) from the New Britain intra-oceanic arc system of Papua New Guinea. A. Quaternary volcanism is divided into 6 zones parallel to the trench (E, F, Gs, Gn, Hs, and Hn) that overlie progressively deeper parts of the subducting slab (BVSP, 1981; Woodhead and Johnson, 1993; Woodhead et al., 1998). B. δ^{56}Fe correlates with TiO_2 concentration, the variations of which have been ascribed to decrease in water flux and degree of partial melting with increasing depth and distance from the trench (Woodhead and Johnson, 1993; Woodhead et al., 1998). Basalts formed by low degrees of partial melting (high TiO_2) have δ^{56}Fe similar to MORBs/OIBs (~+0.1‰) while samples formed by high degrees of partial melting (low TiO_2) have near-chondritic δ^{56}Fe (~0‰). The blue area is the 95% confidence band of linear regression through the data. (For interpretation of the references to colour in this figure legend, the reader is referred to the web version of this article.)

reflects extraction of the most incompatible elements by a prior episode of melting associated with subduction at the now inactive Manus–Kilinailau trench. Across arc trends in chemical compositions (e.g. increase in Ti away from the trench) may be caused by a decrease in the degree of partial melting and fluid flux with depth (Woodhead and Johnson, 1993).

2.2.2.2. Tonga. Four rocks from Hunga Ha'apai, Metis Shoal, and Eua islands were analyzed. They range in compositions from basalt to dacite (from 49.19 to 64.25 wt.% SiO_2). All specimens were provided by the Smithsonian Institution (catalog nos. NMNH 111549-7, 111550-1, 111550-3, and 111108). Melson et al. (1970), Bryan et al. (1972), and Ewart et al. (1973, 1994) reported chemical compositions and petrographic descriptions of these samples. Ewart et al. (1998) discussed in detail existing chemical and isotopic constraints on the evolution of the Tonga–Kermadec arc system.

2.2.2.3. Izu–Mariana. Excluding boninites, 9 rocks from this arc system were studied. The chemical compositions of the 8 samples from the Mariana arc (catalog nos. NMNH 109982-4, 5, 6, 7, 8, 37, 107, and 135) were reported in Tables 5 and 6 of Schmidt (1957). They comprise 5 basalts from Agrihan, Pagan, and Alamagan, as well as 3 andesites from Saipan. The SiO_2 concentrations range from 48.89 to 60.80 wt.%. One sample from the Izu arc (O-shima Island) was studied (NMNH 112960). This basalt (48.02 wt.% SiO_2) was characterized by Kuno (1959) and Tatsumoto and Knight (1969). Stern et al. (2003) provided a detailed description of the Izu–Bonin–Mariana subduction system.

2.2.3. Modern boninites

A total of 21 boninites were selected for this study. A spinel–clinoenstatite–olivine–bronzite boninite from Muko-Jima (Bonin Islands) was provided by the Smithsonian Institution (catalog no. NMNH 116469). Although its chemical composition is unknown, it may be similar to sample #1 in Table 1 of Shiraki et al. (1980). Ohnenstetter and Brown (1996) characterized 4 additional samples from Chichi-Jima, Bonin Islands (780/67a, 780/67c, 780/67g, 780/67h). They are part of a 5-m-thick composite dyke, where sample 780/67h comes from near the center and 780/67a from close to the margin. Of the samples from Népoui (New Caledonia), a clinoenstatite boninite without olivine from a thin dyke (BON 1) was described by Ohnenstetter and Brown (1992, 1996). The chemical compositions of the remaining 15 are reported for the first time in Appendix A (RB 1D, 2, 3, 5, 6, 7, 13, 14, 21, RBP 5, 6, RPQ 1A, RB Pont7, RR 10). Ohnenstetter collected these samples in the Rivière Rouge–Rivière Blanche area, near Népoui. They occur as pillow lavas and massive flows. They are composed of phenocrysts of clinoenstatite and olivine, microphenocrysts of orthopyroxenene with overgrowths of clinopyroxene and amphibole, and microlites of clinopyroxenes and Cr-spinel in a fresh glassy groundmass. These boninites all have low CaO/Al_2O_3 ratios (~0.40), low CaO (~3.6 wt.%), low FeO_{tot} (~7 wt.%), high Al_2O_3 (~9 wt.%) and high alkali contents ($Na_2O + K_2O$ ~2.4 wt.%). According to Crawford et al. (1989), they are classified as type 1 low-Ca boninites. The 4 samples from Chichi-Jima and the sample from Muko-Jima are type 3 low-Ca boninites. As far as boninite petrogenesis is concerned, the samples from New Caledonia may represent an end-member that formed by large water fluxing and high degree of partial melting of a very depleted mantle source (Crawford et al., 1989). The high water content of the melt inhibited feldspar nucleation (Ohnenstetter and Brown, 1992).

2.2.4. Eoarchean igneous rocks

The Eoarchean Itsaq Gneiss Complex of southern West Greenland contains the Isua supracrustal belt (ISB), which is the largest and best-preserved occurrence of ~3.7 and ~3.8 Ga supracrustal rocks on Earth (Nutman et al., 1996, 2002a; Rosing et al., 1996; Myers, 2001; Nutman and Friend, 2009 and references therein). Zircon U–Pb geochronology on Itsaq Gneiss complex samples gives protolith ages that range between ~3.60 and 3.85 Ga. All rocks have been affected by amphibolite or granulite facies metamorphism and have been subjected to variable degrees of metasomatism, deformation, and commonly migmatization. Samples least modified by these secondary processes were targeted for this study. Although the prefix meta is omitted in the following, one should bear in mind that all rocks have been metamorphosed.

2.2.4.1. Amphibolites of IAB chemical affinity. In low-strain domains of the ISB, relict pillow structures indicate that lavas were erupted under water (Maruyama et al., 1992; Nutman et al., 1996; Komiya et al., 1999). Some rocks show strong geochemical similarities to Phanerozoic island arc basaltic-to-picritic volcanic rocks (Polat and Hofmann, 2003; Jenner et al., 2009). A suite of eight ~3.8 Ga IABs from the southern edge of the ISB described by Nutman et al. (1996) and Jenner et al. (2009) were selected for study (G93-35, JG03-40b, -42, -48, -52, -60, -62, and -63). They span a wide range of iron concentrations, from 9 to 16.3 wt.% Fe_2O_3. Other samples of island arc affinity from the ~3.7 Ga northern part of Isua (G04-86, G04-87, G05-32, G05-33, unpublished) and more highly deformed rocks affected by granulite facies from the island of Akilia with an age of ~3.85 Ga (JG03-03, G99-33, Nutman et al., 2009) were also analyzed.

2.2.4.2. Amphibolites of boninite chemical affinity. Polat et al. (2002) recognized the presence of boninite-like volcanic rocks in the ISB. Like their Phanerozoic counterparts, they are characterized by high MgO, Al_2O_3, Ni, and Cr contents but low Ti, Zr, Y and REE concentrations. However, while modern boninites tend to have intermediate compositions (52 to 63 wt.% SiO_2, Crawford et al., 1989), Eoarchean boninites are more basic (45 to 52 wt.% SiO_2; Polat et al., 2002). Three 3.7 Ga volcanic rocks of boninitic affinity were selected for iron isotopic analyses (G04-75, G04-73A, and G04-73B, unpublished).

2.2.4.3. Mafic and ultramafic plutonic rocks. Distinction between metagabbros and metabasalts is based on their field occurrence. Gabbros are often associated with compositionally layered ultramafic rocks that represent the cumulate portion of dismembered igneous intrusions (Dymek et al., 1988; Nutman et al., 1996). Three ~3.8 Ga gabbros and plutonic ultramafic rocks from 5 to 10 km south of Isua were selected for study (G91-87, G97-22, unpublished; G93-72, Friend et al., 2002). We also analyzed 6 samples from ~3.85 Ga layered gabbro and ultramafic enclaves of South-East Qilanngaarsuit island (G91-30, G93-149, G99-21, Nutman et al., 2002b; G01-54, G01-56, G01-84, unpublished).

2.2.4.4. Tonalites. The Itsaq Gneiss Complex is dominated by tonalite–trondhjemite–granodiorite gneisses. Four tonalites were selected for iron isotopic analyses (G97-18 dated at 3.81 Ga, Nutman et al., 1999; G01-113 and G99-22 dated at 3.85 Ga, Nutman et al., 2007; 3.7 dated at 3.7 Ga, unpublished). All these tonalites are well-preserved and their crystallization ages are established by Pb–Pb dating of magmatic zircons.

2.2.4.5. Peridotites of probable mantle origin. Identification of mantle peridotites in highly metamorphosed terranes can be problematic (Friend et al., 2002). Using stringent criteria, Rollinson (2007) reevaluated the mantle peridotite protolith identifications of Friend et al. (2002) and concluded that ~3.8 Ga harzburgite G93-42 and dunite G93-48 were definitely of mantle origin. The unradiogenic ^{187}Os isotopic compositions of these samples further confirm their antiquity (Bennett et al., 2002) and these two samples were selected for study. Additionally, four ~3.7 Ga peridotites from the northern side of the ISB (G05-35, Nutman and Friend, 2009; G07-09, G07-10, G07-35, unpublished) and two 3.85 Ga peridotites from South-East Narssaq (G01-03 and G01-05, unpublished) were analyzed. We wish to caution the reader that the protolith assignment of some of

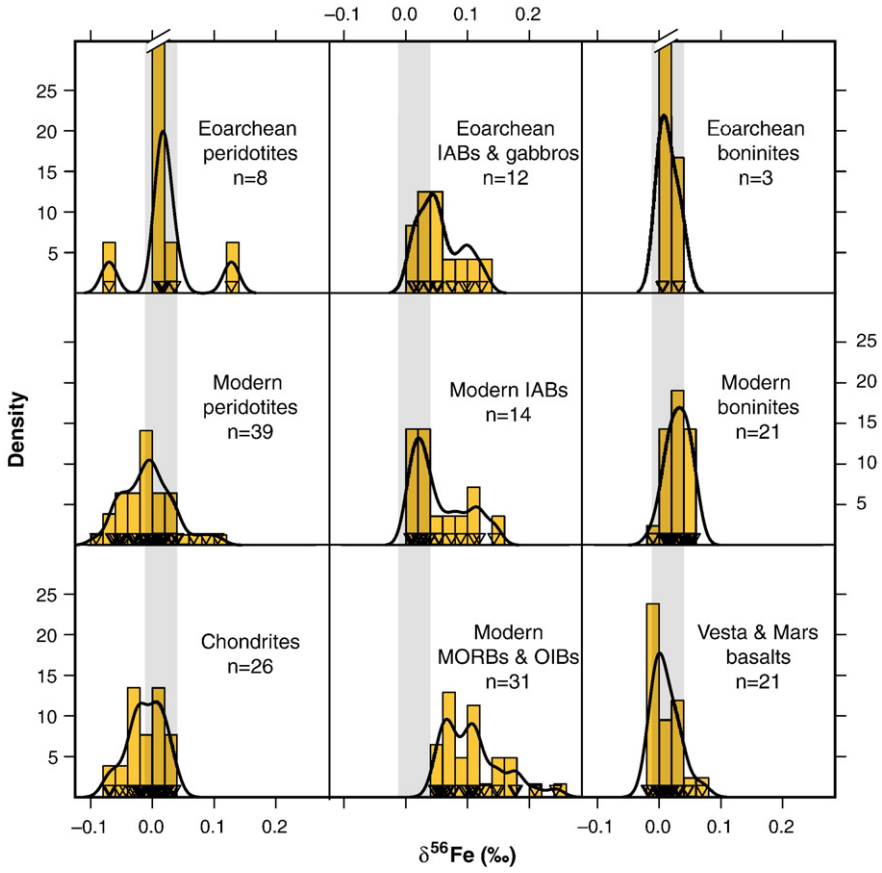

Fig. 3. Iron isotope density distributions of chondrites and igneous rocks from Earth spanning a >3.8 billion year age range (modern and ancient mantle peridotites with Mg# > 0.89, basalts *sensu stricto*, and boninites), Mars (basaltic Shergottites), and asteroid 4 Vesta (Eucrites) (Table 1, Appendix A, Poitrasson et al., 2004, 2005; Weyer et al., 2005; Williams et al., 2005; Anand et al., 2006; Schoenberg and von Blanckenburg, 2006; Weyer and Ionov, 2007; Teng et al., 2008; Schuessler et al., 2009). The grey vertical bar at $\delta^{56}Fe = +0.02 \pm 0.03‰$ is the inferred composition of the fertile upper-mantle (Weyer and Ionov, 2007). While MORBs and OIBs are enriched in the heavy isotopes of Fe (~+0.1‰) relative to chondrites and the fertile upper-mantle, many IABs and most boninites and extraterrestrial basalts have near-chondritic $\delta^{56}Fe$. The inverted triangles are the input (i.e. measured) $\delta^{56}Fe$ values, the vertical yellow bars are normalized histograms (area = 1, bin width = 0.02), the smooth curves are kernel density estimations (Gaussian kernel with bandwidth = 0.013, Bowman and Azzalini, 1997). (For interpretation of the references to colour in this figure legend, the reader is referred to the web version of this article.)

these samples is not without ambiguities and might change in the future as our knowledge increases.

3. Results

Eoarchean peridotites with Mg# > 89 ($n = 8$) overall define a narrow range of compositions, with two outliers (Fig. 3, Table 1, Appendix A). The mode of the distribution ($\delta^{56}Fe \sim 0.02‰$) is identical to the value of the fertile upper-mantle derived from measurements of modern peridotites (Weyer and Ionov, 2007). Modern ($n = 21$) and Eoarchean ($n = 3$) boninites define a narrow range of $\delta^{56}Fe$ values centered at $+0.028 \pm 0.008‰$ ($\pm$95% confidence interval, Table 1, Fig. 3). This is identical to the fertile upper-mantle value of $\sim+0.02 \pm 0.03‰$ (Weyer and Ionov, 2007) or the average composition of basalts from Mars and Vesta ($+0.011 \pm 0.010‰$, $n = 21$) (Poitrasson et al., 2004; Weyer et al., 2005; Anand et al., 2006; Schoenberg and von Blanckenburg, 2006). It is also close to the chondritic value ($-0.010 \pm 0.011‰$, $n = 26$) (Table 1; Poitrasson et al., 2005; Schoenberg and von Blanckenburg, 2006; Teng et al., 2008), yet falls significantly below MORBs and OIBs ($+0.110 \pm 0.018‰$, $n = 31$) (Poitrasson et al., 2004; Schoenberg and von Blanckenburg, 2006; Weyer and Ionov, 2007; Teng et al., 2008; Schuessler et al., 2009). Although both modern ($n = 14$) and Eoarchean ($n = 12$) IABs show $\delta^{56}Fe$ density distributions that peak near the fertile mantle composition, they extend to higher, MORB-like values (up to +0.14‰, Table 1). Dauphas et al. (2004b, 2007a,b) measured Eoarchean mafic and ultramafic rocks that had on average near-chondritic $\delta^{56}Fe$ value but the precision was insufficient to definitely rule out MORB-like composition.

Chondrite groups show little variation in $\delta^{56}Fe$ values (Table 1; Poitrasson et al., 2005, Schoenberg and von Blanckenburg, 2006, Teng

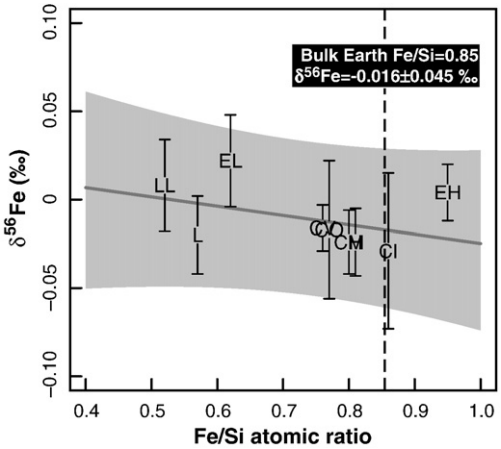

Fig. 4. Average $\delta^{56}Fe$ values of chondritic meteorites (high-precision data from Table 1; Poitrasson et al., 2005; Schoenberg and von Blanckenburg, 2006, Teng et al., 2008). EL6 breccia Blithfield, which shows evidence for iron remobilization (Rubin, 1984) and has anomalously low $\delta^{56}Fe$ value, was excluded from this compilation. At a Fe/Si ratio of 0.85 (Allègre et al., 2001), the bulk Earth is estimated to have $\delta^{56}Fe = -0.016 \pm 0.045$ ‰.

et al., 2008). Based on those measurements, the δ^{56}Fe value of the bulk Earth is estimated to be -0.016 ± 0.045‰ (Fig. 4).

The iron isotopic compositions of basalts from the New-Britain island arc correlate with TiO_2 (Table 1, Appendix A, Fig. 2B), which is an indicator of degree of melting in subduction-zone settings (Stolper and Newman, 1994; Woodhead et al., 1998; Kelley et al., 2006). They also correlate with other fluid-immobile incompatible elements such as Yb (Bézos et al., 2009). Samples near the trench that have received large influx of water from the subducting slab and represent high degree partial melts (e.g. 17%; Woodhead and Johnson, 1993) have compositions similar to the fertile mantle. Samples away from the trench that have received smaller influx of water and represent lower degree partial melts (e.g. 2%; Woodhead and Johnson, 1993) have compositions similar to MORBs.

4. Discussion

As shown in this study, mafic magmas formed by flux melting in subduction-zone settings have variable iron isotopic compositions, ranging from chondritic to +0.15‰ heavier δ^{56}Fe. Hereafter, we discuss the origins of the observed variations and their broader implications for Earth and other terrestrial planets.

4.1. Magmatic differentiation

The removal of low δ^{56}Fe cumulate minerals during magmatic differentiation can drive evolved lavas towards high δ^{56}Fe values (Teng et al., 2008; Schuessler et al., 2009). However, this process cannot explain the isotopic variations reported here because all IABs, MORBs, and OIBs plotted in Fig. 3 are basalts sensu stricto (45–52 wt.% SiO_2, <5 wt.% $Na_2O + K_2O$) and no correlation is found between δ^{56}Fe values and indicators of magmatic differentiation (e.g. MgO, Appendix A) within this narrow range of composition. The correlation between δ^{56}Fe and TiO_2, an indicator of degree of partial melting (Fig. 2B) in New Britain IABs, is further evidence that the observed variations reflect source-related processes. The few near-chondritic δ^{56}Fe values previously found in terrestrial magmatic rocks containing over 20 wt.% MgO (compared to 4.45–10.80 wt.% for IABs in Fig. 3) are due to olivine accumulation (Teng et al., 2008). Boninites are rich in MgO but do not result from olivine accumulation. Rather, they are the product of high degree partial melting of depleted sources at relatively low pressure in the presence of water (Crawford et al., 1989).

4.2. Mantle metasomatism

Metasomatism is another process that can modify the iron isotopic composition of mantle material (Beard and Johnson, 2004; Williams et al., 2005; Weyer and Ionov, 2007). For example, sub-arc peridotites show large variations in δ^{56}Fe, with values as low as −0.56‰ documented (Williams et al., 2005). This could reflect kinetic isotope fractionation associated with diffusion of iron from melts percolating through peridotite (Weyer and Ionov, 2007) or mixing with slab-derived melts enriched in the light isotopes of iron (e.g. δ^{56}Fe = −3‰) (Beard and Johnson, 2004; Williams et al., 2005). However, several lines of evidence argue against these processes as the main cause for the isotopic variations documented here. First, the density distributions of δ^{56}Fe in IABs and boninites peak at the inferred value of the fertile upper-mantle (Fig. 3). If interpreted in terms of metasomatism, this would require that fluid or magma interaction shifts the δ^{56}Fe value of the mantle wedge by an exact quantity to produce fractionated magmas with the composition of the fertile upper-mantle. Such a scenario seems implausible. Second, one might expect metasomatism to produce a wider range of iron isotopic compositions (e.g. as is observed in metasomatized peridotites, Beard and Johnson, 2004; Williams et al., 2005; Weyer and Ionov, 2007). The opposite is true for the boninites analyzed in this study (Fig. 3); boninites show a narrower range of δ^{56}Fe values ($\sigma = 0.018$ ‰, reduced $\chi^2 = 1.2$ entirely explained by analytical uncertainty) than MORBs and OIBs ($\sigma = 0.049$‰, reduced $\chi^2 = 24$). However, part of the dispersion in δ^{56}Fe values of MORBs and OIBs reported in previous studies (Poitrasson et al., 2004; Schoenberg and von Blanckenburg, 2006; Weyer and Ionov, 2007; Teng et al., 2008; Schuessler et al., 2009) might be due to inter-laboratory bias and non-representativeness of the samples selected. The arguments presented here against metasomatism are mostly circumstantial, so one cannot exclude definitively the possibility that transfer of isotopically light Fe^{3+}-bearing water-rich fluids from the subducting slab to the mantle wedge induced melting, which might explain the correlation between δ^{56}Fe and degree of partial melting seen in New Britain island arc.

4.3. Redox-controlled iron isotopic fractionation during melting

Iron isotopic fractionation associated with melting (Weyer et al., 2005; Williams et al., 2005, 2009; Schoenberg and von Blanckenburg, 2006; Weyer and Ionov, 2007) appears to be the most likely mechanism for explaining the observed isotopic variations in mantle-derived magmatic rocks. Weyer and Ionov (2007) suggested that a correlation between δ^{56}Fe and Mg# in mantle peridotites, reflected a constant ~+0.1‰ iron isotopic fractionation between liquid and solid and a near-chondritic iron isotopic composition for the silicate Earth (δ^{56}Fe~ + 0.02‰ at Mg# = 0.894). These values were obtained by including mantle peridotites showing signs of metasomatism (Fig. 3A of Weyer and Ionov, 2007). If one excludes those samples, the δ^{56}Fe value of the fertile mantle increases to ~+0.05‰ but the correlation with Mg# is even steeper, corresponding to ~+0.3‰ iron isotopic fractionation between liquid and solid (Fig. 3B of Weyer and Ionov, 2007). Accordingly, one cannot explain the peridotite data presented by Weyer and Ionov (2007) by a fertile mantle δ^{56}Fe value of +0.1 ‰ and negligible isotopic fractionation during melting, as some have suggested.

A difficulty with the idea that there is constant iron isotopic fractionation between liquid and solid is that it does not readily explain why basalts from Mars and Vesta have near-chondritic Fe isotopic compositions (Poitrasson et al., 2004; Weyer et al., 2005; Anand et al., 2006; Schoenberg and von Blanckenburg, 2006). It also cannot explain why all boninites and many IABs have compositions identical to the fertile upper-mantle (Fig. 3). Indeed, assuming a constant liquid–solid isotopic fractionation in Fe isotopes, one would not expect to see much change in δ^{56}Fe values of magmas generated over a large melting interval (up to 40%) (Williams et al., 2005; Weyer and Ionov, 2007).

These caveats led us to explore quantitatively the possibility that the observed isotopic variations are primarily controlled by equilibrium fractionation between Fe^{2+} and Fe^{3+} during mantle melting (Appendix B). As is the case for equilibrium fractionation between phases, one can write an isotope exchange reaction between oxidation states: $^{54}Fe^{2+} + {}^{56}Fe^{3+} \leftrightarrows {}^{56}Fe^{2+} + {}^{54}Fe^{3+}$. Because Fe^{3+} is more incompatible than Fe^{2+} during partial melting (by a factor of ~10, Canil et al., 1994; Woodland et al., 2006) and given that ferric iron usually has higher δ^{56}Fe than ferrous iron (e.g. Polyakov and Mineev, 2000; Polyakov et al., 2007; Schuessler et al., 2007; Shahar et al., 2008; Schoenberg et al., 2009), one would expect the liquid to be enriched in the heavy isotopes of iron relative to the solid residue (Williams et al., 2005; Weyer and Ionov, 2007). Based on this hypothesis, we develop the first quantitative model that relates the iron isotopic composition of magmas to the degree of partial melting, Fe^{3+}/Fe^{2+} ratio, and buffering capacity of the mantle (Appendix B).

Equilibrium isotopic fractionation between Fe^{2+} and Fe^{3+} in solid and liquid silicates at mantle temperature is not known experimentally. However, nuclear inelastic resonant X-ray scattering and Mössbauer spectroscopy of ^{57}Fe can predict iron isotopic fractionation both between minerals and within minerals between crystallographic sites (Polyakov and Mineev, 2000; Polyakov et al., 2007; Schoenberg et al., 2009). In all silicates studied by Polyakov and Mineev (2000)

and Schoenberg et al. (2009), there is a systematic difference between the β-factors (reduced isotopic partition function ratio) of Fe^{2+} and Fe^{3+}, but little variation from one mineral or site to another for a given oxidation state and coordination number (i.e. $10^3\ln\beta_{Fe^{3+}} - 10^3\ln\beta_{Fe^{2+}} > 0$; $10^3\ln\beta_{Fe^{3+}}$, $10^3\ln\beta_{Fe^{2+}}$ ~constant for 6-fold coordination, Fig. 5). This is true both between and within minerals (Fe^{2+} in olivine, enstatite, and hedenbergite; Fe^{3+} in aegirine; Fe^{2+} and Fe^{3+} in diopside and riebeckite), which can be summarized as $10^3\ln\beta_{Fe^{3+}mineral} \approx 75\times10^4/T^2$, $10^3\ln\beta_{Fe^{2+}mineral} \approx 34\times10^4/T^2$, and $10^3\ln\beta_{Fe^{3+}mineral} - 10^3\ln\beta_{Fe^{2+}mineral} \approx 41\times10^4/T^2$ (T in K). As expected, the magnitude of the fractionation decreases with increasing temperature ($\propto 1/T^2$) but it is still significant at temperatures relevant to mantle melting (e.g. ~0.2‰ at 1200 °C).

Schuessler et al. (2007) carried out experiments that can be used to indirectly estimate the β-factor for Fe^{3+} in peralkaline rhyolitic melt. They measured iron isotopic fractionation between pyrrhotite and peralkaline rhyolitic melt containing 62% Fe^{3+} and 38% Fe^{2+}. Between 840 and 1000 °C, the experiments revealed approximately constant ~+0.35 ‰ fractionation between pyrrhotite and melt, corresponding to $10^3\ln\beta_{melt} - 10^3\ln\beta_{pyrrhotite} \approx 50\times10^4/T^2$. This result can be combined with the β-factor for pyrrhotite derived by Polyakov et al. (2007) from nuclear inelastic resonant X-ray scattering ($10^3\ln\beta_{pyrrhotite} \approx 29\times10^4/T^2$) to estimate the β-factor for the silicate melt, $10^3\ln\beta_{melt} \approx 79\times10^4/T^2$. This β-factor is the average of the contribution from 38% Fe^{2+} and 62% Fe^{3+}. Assuming that Fe^{2+} in the melt has the same β-factor as Fe^{2+} in silicate minerals (i.e., $\approx 34\times10^4/T^2$), one can derive for the β-factor of Fe^{3+} in a melt of peralkaline rhyolitic composition, $10^3\ln\beta_{Fe^{3+}melt} \approx 107\times10^4/T^2$ (Fig. 5). This would correspond to a fractionation between Fe^{2+} and Fe^{3+} of ~+0.3‰ in melt at 1200 °C, possibly higher than what was estimated for silicate minerals (~+0.2‰ at the same temperature). However, the coordination environments of Fe^{2+} and Fe^{3+} in rhyolitic and basaltic melt may be different (e.g. Métrich et al., 2006, Mysen, 2006; Schuessler et al., 2007), which could affect β-factors, so further experimental work is needed. As a first approach we assume that the β-factors of Fe^{2+} and Fe^{3+} in silicate liquid and solid are identical (Appendix B).

We have calculated evolution curves for δ^{56}Fe by assuming equilibrium isotope fractionation between Fe^{2+} and Fe^{3+} and preferential extraction during melting of heavier, incompatible Fe^{3+} (Fig. 6, Appendix B). The Fe^{3+}/Fe^{2+} ratio of MORBs shows little variation over 5–20% partial melting (Christie et al., 1986; Bézos and Humler, 2005; Frost and McCammon, 2008), suggesting that oxygen fugacity is buffered during melting. The chemical agent responsible for such buffering is uncertain but the mineral composition of the source could have played a role. As the degree of melting increases during MORB generation, the modal abundance of pyroxene decreases while that of olivine increases. A corresponding increase in the effective melt–solid distribution coefficient of Fe^{3+} is expected, which could have balanced the decrease in the Fe^{3+}/Fe^{2+} ratio of the solid residue, to produce magmas that have approximately constant Fe^{3+}/Fe^{2+} ratio. In order to explain the MORB value of around +0.09‰ (Beard et al., 2003; Poitrasson et al., 2004; Schoenberg and von Blanckenburg, 2006; Weyer and Ionov, 2007) with 10% partial melting (Klein and Langmuir, 1987) of a buffered source characterized by $Fe^{3+}/Fe^{2+} = 0.037$ (Canil et al., 1994) and $\delta^{56}Fe_{source} = +0.02$‰ (Weyer and Ionov, 2007), equilibrium fractionation between Fe^{2+} and Fe^{3+} of ~+0.3‰ is required (Fig. 6A). This is in reasonable agreement with theoretical predictions (Fig. 5).

The amount of moderately incompatible Fe^{3+} left in the residue during non-buffered melting decreases more rapidly than compatible Fe^{2+}. This results in a decrease in the degree of Fe isotope fractionation between liquid and solid. Depleted mantle would be expected to have low Fe^{3+}/Fe^{2+} ratio as a result of preferential extraction of Fe^{3+} (e.g. Fe^{3+}/Fe^{2+}=0.019 instead of 0.037 after 10%

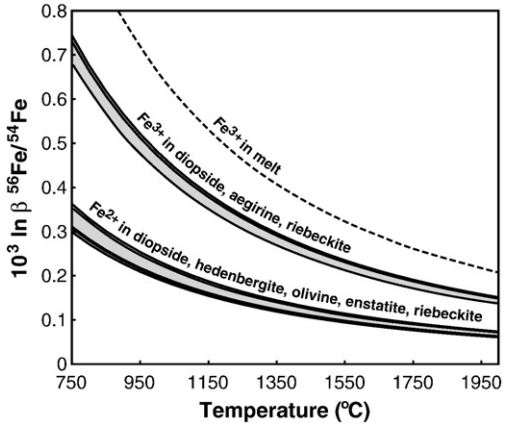

Fig. 5. Reduced isotopic partition function ratios (β-factors, given here for $^{56}Fe/^{54}Fe$) of Fe^{2+} and Fe^{3+} in silicate minerals (Polyakov and Mineev, 2000; Schoenberg et al., 2009) and Fe^{3+} in silicate melt of peralkaline rhyolitic composition (indirect estimate derived from the studies of Schuessler et al., 2007; Polyakov et al., 2007; see text for details). Ferric iron is systematically heavier than ferrous iron (by up to a few tenths of permil at temperatures relevant to magma genesis).

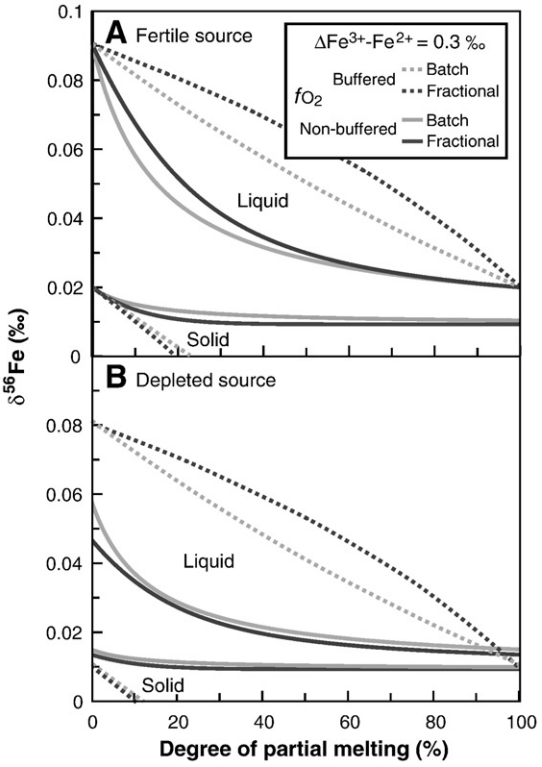

Fig. 6. Redox-controlled Fe isotope fractionation of fertile (A) and depleted (B) mantle sources (the relevant equations are given in Appendix B). Equilibrium fractionation between Fe^{2+} and Fe^{3+} is taken to be $\Delta Fe^{3+} - Fe^{2+} = +0.3$‰ (Fig. 5). The liquid/solid distribution coefficients of Fe^{2+} and Fe^{3+} are 1 and 10, respectively (Canil et al., 1994). Because Fe^{3+} is more incompatible than Fe^{2+}, the liquid has higher Fe^{3+}/Fe^{2+} than the solid residue and hence higher δ^{56}Fe. The initial Fe^{3+}/Fe^{2+} and δ^{56}Fe of the fertile mantle are 0.037 and +0.02‰, respectively (Canil et al., 1994; Weyer and Ionov, 2007). For buffered melting, the Fe^{3+}/Fe^{2+} ratio of the solid residue remains constant (0.037), corresponding to usual equations of isotopic fractionation upon melting with $\Delta liquid - solid = +0.07$‰. For non-buffered melting, as melt extraction progresses the amount of Fe^{3+} left in the residue decreases and isotopic fractionation between liquid and solid also decreases. The starting parameters for non-buffered melting of a depleted source are from fertile mantle after 10% non-buffered melt extraction. MORB/OIB δ^{56}Fe values can be explained by small to moderate degrees of partial melting of a source with Fe^{3+}/Fe^{2+} ~0.037 (e.g. 10% buffered fractional melting in A). Many IABs and most boninites have δ^{56}Fe similar to the mantle because they formed from larger degrees of partial melting of depleted mantle sources with Fe^{3+}/Fe^{2+} ~0.02 (e.g. 20% non-buffered fractional melting in B).

melt extraction). Non-buffered melting of such sources would yield minimal iron isotopic fractionation (compare Figs. 6A and B). Thus, boninite δ^{56}Fe values of ~+0.03‰ can be explained by 20% melting of a non-buffered source previously depleted by 10% non-buffered melt extraction. A possible reason for the lack of buffering of oxygen fugacity during boninite genesis might be the low modal abundance of pyroxene in the harzburgitic source that would otherwise act as an internal buffer. The factors affecting the iron isotopic composition of subduction-related magmas appear intimately related to the oxygen fugacity of the mantle (i.e., Fe^{3+}/Fe^{2+} ratio). Although arc peridotites and basalts are oxidized (Parkinson and Arculus, 1999; Frost and McCammon, 2008; Kelley and Cottrell, 2009), this may reflect secondary alteration in the lithosphere or during degassing (Lee et al., 2005). Indeed, V/Sc ratios in arc samples typically record MORB-like oxygen fugacity during magma genesis (Lee et al., 2005). The near-chondritic δ^{56}Fe values of boninites and some IABs of both Eoarchean and Phanerozoic ages are consistent with low Fe^{3+}/Fe^{2+} ratios (e.g. ~0.02) in their source regions.

The simple model presented here predicts much higher Fe^{3+}/Fe^{2+} ratio in MORB-type magmas than what is observed (i.e., Fe^{3+}/Fe^{2+}~0.14; Bézos and Humler, 2005). For instance, for 10% non-buffered fractional melting, the fractionation in δ^{56}Fe value between the cumulative melt and the residue is ~+0.06‰ but the corresponding Fe^{3+}/Fe^{2+} ratio in the melt is 0.24. This discrepancy could be alleviated using a lower initial Fe^{3+}/Fe^{2+} ratio or lower melt–solid distribution coefficient for Fe^{3+} if (1) Fe^{2+} in basaltic melts was isotopically heavier than Fe^{2+} in mantle minerals, (2) Fe^{3+}–Fe^{2+} fractionation in silicate melts was larger than the value adopted here (+0.3‰), and (3) the iron isotopic difference between MORB and mantle was smaller than what was adopted here. In addition to oxidation state, iron coordination environment may affect iron isotopic fractionation (e.g., Polyakov and Mineev, 2000; Schauble, 2004). For instance, the ~0.15‰ difference in δ^{56}Fe value between high Ti and low Ti lunar mare basalts (Poitrasson et al., 2004; Weyer et al., 2005) cannot be related to redox conditions as Fe^{3+} is virtually absent from the Moon. Instead, crystallization from silicate melts of more exotic phases like ilmenite ($Fe^{2+}TiO_3$) might have induced iron isotopic fractionation. Such considerations are important for isotopic fractionation between Fe^{2+} and Fe^{3+} in silicate melts (e.g. Schuessler et al., 2007). In silicate minerals, Fe^{2+} and Fe^{3+} are usually in 6-fold coordination with oxygen. In basaltic melts, the effective coordination of Fe^{2+} and Fe^{3+} is about 5, with Fe^{3+} possibly in a slightly lower coordination than Fe^{2+} (e.g., Jackson et al., 2005; Wilke et al., 2005; Métrich et al., 2006). It is unknown how the 5-fold coordination, which represents an average, is actually distributed between 4-, 5- and 6-fold coordination polyhedra. All things equal, iron is expected to be isotopically heavier in lower coordination environments. Thus, differences in iron coordination between melt and solid may enhance the isotopic fractionation between minerals and melt associated with redox.

4.4. Perspectives for redox conditions in Mars and the early Earth

Iron isotopes can also provide important constraints on the Fe^{3+}/Fe^{2+} ratio in the early Earth. The peak in the distribution of δ^{56}Fe values of Eoarchean mantle peridotites at the value of the fertile upper-mantle (Fig. 3) is consistent with no significant change in the iron isotopic composition of Earth's mantle for more than 3.8 billion years. A notable feature of some Eoarchean IABs and gabbros is that they have heavy iron isotopic compositions around +0.1 ‰ (e.g. JG03-60, JG03-63, G04-86, G04-87, Table 1), which are difficult to interpret if Earth's mantle at 3.8 Ga was significantly more reduced (lower Fe^{3+}/Fe^{2+}) than at present. In Fig. 7, iron isotopic fractionation between melt and source is calculated for a range of initial Fe^{3+}/Fe^{2+} ratios. If correct, this calculation shows that some regions of Earth's mantle at 3.8 Ga had Fe^{3+}/Fe^{2+} ratios similar to modern values (~0.037, Canil et al., 1994) in order to explain the heavy iron isotopic composition of certain Eoarchean basalts. This agrees with the studies of Canil (1997), Delano (2001), Li and Lee (2004), and Berry et al. (2008) who showed that the oxygen fugacities during mafic and ultramafic magmatism at 2.7–3.5 Ga were close to those of modern basalts.

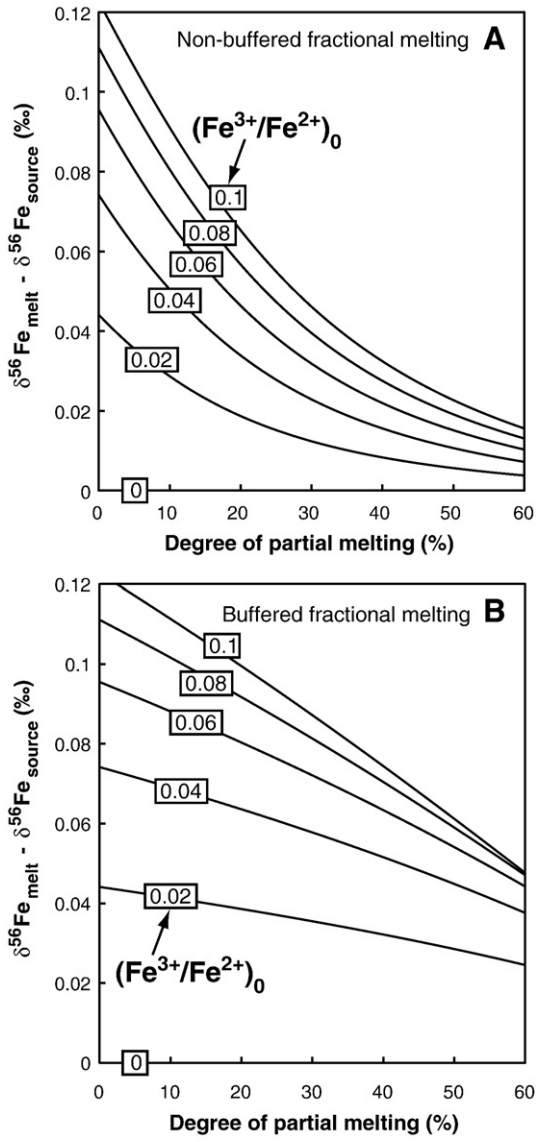

Fig. 7. Calculation of melt-source iron isotopic fractionation as a function of degree of partial melting and initial Fe^{3+}/Fe^{2+} ratios. A. Non-buffered fractional melting. B. Buffered fractional melting. The following parameters were adopted: $\Delta Fe^{3+}-Fe^{2+}$ = +0.3‰, KFe^{2+}=1, KFe^{3+}=10. See text and Appendix B for details.

The idea that iron isotopic fractionation may be controlled by equilibrium fractionation between Fe^{2+} and Fe^{3+} deduced from the terrestrial basalt and boninite data presented here can also explain why basaltic meteorites from Mars and Vesta have near-chondritic iron isotopic compositions (Poitrasson et al., 2004; Weyer et al., 2005; Anand et al., 2006; Schoenberg and von Blanckenburg, 2006). The parent body of Eucrites is relatively reduced (oxygen fugacity at one log unit below Iron-Wüstite buffer, IW-1) (Wadhwa, 2008 and references therein) compared to Earth's upper-mantle (~IW+3.5). Basaltic shergottites also formed under low oxygen fugacity (IW-1 to IW+2.5). The most oxidized compositions among these martian meteorites may reflect interaction between melts derived from a reduced mantle source (~IW-1) and oxidized crust (e.g. Wadhwa, 2001, 2008; Herd et al. 2002). Indeed, in these samples oxidation fugacity correlates with initial strontium and neodymium isotopic compositions, possibly reflecting processes of crustal assimilation. The relevant oxygen fugacity during genesis of basaltic shergottites may

therefore be ~ IW-1. According to our model, partial melting of reduced mantle on Mars and Vesta (IW-1, Fe^{3+}/Fe^{2+}~0) would produce magmas with iron isotopic composition identical to the source, $\delta^{56}Fe_{melt}-\delta^{56}Fe_{source}\propto(Fe^{3+}/Fe^{2+})_0$ (Appendix B, Fig. 7), consistent with the fact that these meteorites have near-chondritic $\delta^{56}Fe$ values.

5. Conclusions

It was previously suggested that all terrestrial mantle-derived magmas had heavy iron isotopic composition relative to chondrites ($\delta^{56}Fe\sim+0.1$ ‰). New results reported here show that many Eoarchean (≥3.7 Ga) to modern boninites and island arc basalts (IABs) formed by large degrees of flux melting of depleted mantle sources have near-chondritic iron isotopic compositions ($\delta^{56}Fe\sim+0.03$‰, Fig. 3). In the New-Britain island arc, $\delta^{56}Fe$ correlates with TiO_2, a proxy for degree of partial melting (Fig. 2). These variations are best explained by ~0.3‰ equilibrium isotope fractionation between Fe^{2+} and Fe^{3+} during mantle melting to form oceanic crust, with preferential extraction of isotopically heavier, incompatible Fe^{3+}. A quantitative model that relates the iron isotopic composition of magmas to the degree of partial melting, Fe^{3+}/Fe^{2+} ratio (i.e., redox conditions), and buffering capacity of the mantle is presented for the first time (Appendix B). The idea that iron isotopic fractionation during melting may be controlled by equilibrium fractionation between Fe^{2+} and Fe^{3+} has important implications:

1. The heavy iron isotopic composition of Earth's oceanic crust relative to basalts from Mars and Vesta is related to the oxidized nature of Earth's mantle (IW + 3.5 for Earth versus IW-1 for Mars and Vesta).
2. Heavy iron isotopic compositions measured in some Eoarchean basalts (up to ~+0.1‰, similar to modern MORBs and OIBs) suggests that some regions of Earth's mantle had a Fe^{3+}/Fe^{2+} ratio similar to the modern value (~0.037) at ~3.8 Ga.
3. Subduction-related magmas are derived from regions of the mantle that have Fe^{3+}/Fe^{2+} ratios similar to, or lower than, those of mid-ocean ridge sources.
4. The oxidized nature of some martian meteorites reflects modification after melting (e.g. through assimilation) as these samples have chondritic and unfractionated iron isotopic compositions.

The model proposed here is experimentally testable, by measuring iron isotopic fractionation between Fe^{2+} and Fe^{3+} in silicate melts and minerals.

Acknowledgements

Discussions with J.M. Eiler, M. Roskosz, E.M. Stolper, K.A. Farley, F.-Z. Teng, R. Yokochi, V.B. Polyakov and A. Pourmand, careful reviews by F. Poitrasson and E.A. Schauble, as well as comments by editor R.W. Carlson, were greatly appreciated. This work was supported by a Packard fellowship, the France Chicago Center, a Moore Distinguished Scholarship at the California Institute of Technology, and NASA through grants NNG06GG75G and NNX09AG59G to N.D. S.S. Sorensen, Smithsonian Institution, generously provided some boninite and island arc basalt samples.

Appendix A. Supplementary data

Supplementary data associated with this article can be found, in the online version, at 10.1016/j.epsl.2009.09.029.

Appendix B. Redox-driven isotopic fractionation associated with partial melting

The following equations give the Fe isotopic compositions of the liquid (subscript *l* for batch melting or *cl* – cumulative liquid – for fractional melting) and solid (*s*) assuming that Fe isotopic fractionation during melting is solely driven by fractionation between Fe^{2+} and Fe^{3+} (detailed derivation of these equations is given in Appendix A),

$$(^{56}Fe^{3+}/^{54}Fe^{3+})_l/(^{56}Fe^{3+}/^{54}Fe^{3+})_s=(^{56}Fe^{2+}/^{54}Fe^{2+})_l/(^{56}Fe^{2+}/^{54}Fe^{2+})_s=1,$$

$$(^{56}Fe^{3+}/^{54}Fe^{3+})_{l,s}/(^{56}Fe^{2+}/^{54}Fe^{2+})_{l,s}=\alpha.$$

The following notations are used,

$$K=[Fe^{2+}]_l/[Fe^{2+}]_s,$$

$$\beta=(Fe^{3+}/Fe^{2+})_l/(Fe^{3+}/Fe^{2+})_s,$$

$$r=Fe^{3+}/Fe^{2+},$$

$$f=m_l/m_0=1-m_s/m_0,$$

$$\delta=(R/R_{std}-1)\times10^3,$$

$$\Delta=(\alpha-1)\times10^3.$$

a. *Non-buffered batch melting*

$$\delta_s=\delta_0-\frac{r_0}{r_0+1}\times\frac{fK}{(1-f)(r_0+1)+fK(r_0+\beta)}(\beta-1)\Delta$$

$$\delta_l=\delta_0+\frac{r_0}{r_0+1}\times\frac{1-f}{(1-f)(\beta r_0+1)+fK\beta(r_0+1)}(\beta-1)\Delta$$

b. *Non-buffered fractional melting*

$$\delta_s=\delta_0+\frac{r_0}{1+r_0}\times\frac{(1-f)^{K(\beta-1)}-1}{1+r_0(1-f)^{K(\beta-1)}}\times\Delta$$

$$\delta_{cl}=\delta_0-\left(\frac{r_0}{1+r_0}\right)\frac{(1-f)^{\beta K}-(1-f)^K}{1+r_0-(1-f)^K-r_0(1-f)^{\beta K}}\times\Delta$$

c. *Buffered batch melting*

$$\delta_s=\delta_0-\frac{r_0}{r_0+1}\times\frac{fK}{(1-f)(r_0+1)+fK(1+\beta r_0)}\times(\beta-1)\Delta$$

$$\delta_l=\delta_0+\frac{r_0}{r_0\beta+1}\times\frac{1-f}{(1-f)(r_0+1)+fK(1+\beta r_0)}\times(\beta-1)\Delta$$

d. *Buffered fractional melting*

$$\delta_s=\delta_0+\ln(1-f)\ \frac{r_0K}{(1+r_0)^2}(\beta-1)\Delta$$

$$\delta_{cl}=\delta_0-\frac{(1-f)^{K(1+\beta r_0)/(1+r_0)}}{1-(1-f)^{K(1+\beta r_0)/(1+r_0)}}\ln(1-f)\ \frac{r_0K}{(1+r_0)^2}(\beta-1)\Delta$$

References

Allègre, C., Manhès, G., Lewin, E., 2001. Chemical composition of the Earth and volatility control on planetary genetics. Earth Planet. Sci. Lett. 185, 49–69.

Anand, M., Russell, S.S., Blackhurst, R.L., Grady, M.M., 2006. Searching for signatures of life on Mars: an Fe-isotope perspective. Philos. Trans. R. Soc. Lond., B 361, 1715–1720.

Arnold, G.L., Weyer, S., Anbar, A.D., 2004. Fe isotope variations in natural materials measured using high mass resolution multiple collector ICPMS. Anal. Chem. 76, 322–327.

Beard, B.L., Johnson, C.M., 1999. High precision iron isotope measurements of terrestrial and lunar materials. Geochim. Cosmochim. Acta 63, 1653–1660.

Beard, B.L., Johnson, C.M., 2004. Inter-mineral isotope variations in mantle-derived rocks and implications for the Fe geochemical cycle. Geochim. Cosmochim. Acta 68, 4727–4743.

Beard, B.L., Johnson, C.M., 2007. Comment on "Iron isotope fractionation during planetary differentiation" by Weyer et al. Earth Planet. Sci. Lett. 240, 251–264.

Beard, B.L., Johnson, C.M., Skulan, J.L., Nealson, K.H., Cox, L., Sun, H., 2003. Application of Fe isotopes to tracing the geochemical and biological cycling of Fe. Chem. Geol. 195, 87–117.
Bennett, V.C., Nutman, A.P., Esat, T., 2002. The osmium mantle evolution curve and limits on accretion and differentiation of the Earth from Archean (3.4–3.8 Ga) ultramafic rocks. Geochim. Cosmochim. Acta 66, 2615–2630.
Berry, A.J., Danyushevsky, L.V., O'Neill, H., St, C., Newville, M., Sutton, S.R., 2008. Oxidation state of iron in komatiitic melt inclusions indicates hot Archaean mantle. Nature 455, 960–963.
Bézos, A., Humler, E., 2005. The Fe3+/Fe ratios of MORB glasses and their implications for mantle melting. Geochim. Cosmochim. Acta 69, 711–725.
Bézos, A., Escrig, S., Langmuir, C.H., Michael, P.J., Asimow, P.D., 2009. Origins of chemical diversity of back-arc basin basalts: a segment scale study of the Northern Eastern Lau Spreading Center. J. Geophys. Res. 114, B06212. doi:10.1029/2008JB005924.
Bowman, A.W., Azzalini, A., 1997. Applied Smoothing Techniques For Data Analysis: The Kernel Approach With S-Plus Illustrations. Oxford University Press, Oxford.
Bryan, W.B., Stice, G.D., Ewart, A., 1972. Geology, petrography, and geochemistry of the volcanic islands of Tonga. J. Geophys. Res. 77, 1566–1585.
BVSP-Basaltic Volcanism Study Project, 1981. Basaltic Volcanism on the Terrestrial Planets. Pergamon Press, Inc., New York. 1286 pp.
Canil, D., 1997. Vanadium partitioning and the oxidation state of Archaean komatiite magmas. Nature 389, 842–845.
Canil, D., O'Neill, H., St, C., Pearson, D.G., Rudnick, R.L., McDonough, W.F., Carswell, D.A., 1994. Ferric iron in peridotites and mantle oxidation states. Earth Planet. Sci. Lett. 123, 205–220.
Christie, D.M., Carmichael, I.S.E., Langmuir, C.H., 1986. Oxidation states of mid-ocean ridge basalt glasses. Earth Planet. Sci. Lett. 79, 397–411.
Crawford, A.J., Falloon, T.J., Green, D.H., 1989. Classification, petrogenesis and tectonic setting of boninites. In: Crawford, A.J. (Ed.), boninites. Unwin Hyman, London, pp. 1–49.
Dauphas, N., Rouxel, O., 2006. Mass spectrometry and natural variations of iron isotopes. Mass Spectrom. Rev. 25, 515–550 Erratum 25, 831–832.
Dauphas, N., Janney, P.E., Mendybaev, R.A., Wadhwa, M., Richter, F.M., Davis, A.M., van Zuilen, M., Hines, R., Foley, C.N., 2004a. Chromatographic separation and multi-collection-ICPMS analysis of iron. Investigating mass-dependent and -independent isotope effects. Anal. Chem. 76, 5855–5863.
Dauphas, N., van Zuilen, M., Wadhwa, M., Davis, A.M., Marty, B., Janney, P.E., 2004b. Clues from iron isotope variations on the origin of early Archaean banded iron formations from Greenland. Science 306, 2077–2080.
Dauphas, N., Cates, N.L., Mojzsis, S.J., Busigny, V., 2007a. Identification of chemical sedimentary protoliths using iron isotopes in the >3750 Ma Nuvvuagittuq supracrustal belt, Canada. Earth Planet. Sci. Lett. 254, 358–376.
Dauphas, N., van Zuilen, M., Busigny, V., Lepland, A., Wadhwa, M., Janney, P.E., 2007b. Iron isotope, major and trace element characterization of early Archean supracrustal rocks from SW Greenland: protolith identification and metamorphic overprint. Geochim. Cosmochim. Acta 71, 4745–4770.
Dauphas, N., Pourmand, A., Teng, F.-Z., 2009. Routine isotopic analysis of iron by HR-MC-ICPMS: how precise and how accurate? Chem. Geol. 267, 175–184.
Delano, J.W., 2001. Redox history of the Earth's interior since 3900 Ma: implications for prebiotic molecules. Orig. Life Evol. B. 31, 311–341.
Dymek, R.F., Brothers, S.C., Schiffries, C.M., 1988. Petrogenesis of ultramafic metamorphic rocks from the 3800 Ma Isua Supracrustal Belt, West Greenland. J. Petrol. 29, 1353–1397.
Ewart, A., Bryan, W.B., Gill, J.B., 1973. Mineralogy and geochemistry of the younger volcanic islands of Tonga, S.W. Pacific. J. Petrol. 14, 429–465.
Ewart, A., Bryan, W.B., Chappell, B.W., Rudnick, R.L., 1994. 24. Regional geochemistry of the Lau–Tonga arc and backarc systems. Proceedings of the Ocean Drilling Program: Scientific Results, vol. 135, pp. 385–425.
Ewart, A., Collerson, K.D., Regelous, M., Wendt, J.I., Niu, Y., 1998. Geochemical evolution within the Tonga–Kermadec–Lau arc–back-arc systems: the role of varying mantle wedge composition in space and time. J. Petrol. 39, 331–368.
Friend, C.R.L., Bennett, V.C., Nutman, A.P., 2002. Abyssal peridotites >3, 800 Ma from southern West Greenland: field relationships, petrography, geochronology, whole-rock and mineral chemistry of dunite and harzburgite inclusions in the Itsaq Gneiss Complex. Contrib. Mineral. Petrol. 143, 71–92.
Frost, D.J., McCammon, C.A., 2008. The redox state of Earth's mantle. Annu. Rev. Earth Planet. Sci. 36, 389–420.
Gill, J.B., Morris, J.D., Johnson, R.W., 1993. Timescale for producing the geochemical signature of island arc magmas: U–Th–Po and Be–B systematics in recent Papua New Guinea lavas. Geochim. Comochim. Acta 57, 4269–4283.
Heimann, A., Beard, B.L., Johnson, C.M., 2008. The role of volatile exsolution and sub-solidus fluid/rock interactions in producing high $^{56}Fe/^{54}Fe$ ratios in siliceous igneous rocks. Geochim. Cosmochim. Acta 72, 4379–4396.
Herd, C.D.K., Borg, L.E., Jones, J.H., Papike, J.J., 2002. Oxygen fugacity and geochemical variations in the martian basalts: implications for martian basalt petrogenesis and the oxidation state of the upper mantle of Mars. Geochim. Cosmochim. Acta 66, 2025–2036.
Jackson, W.E., Farges, F., Yeager, M., Mabrouk, P.A., Rossano, S., Waychunas, G.A., Solomon, E.I., Brown, G.E., 2005. Multi-spectroscopic study of Fe(II) in silicate glasses: implications for the coordination environment of Fe(II) in silicate melts. Geochim. Cosmochim. Acta 69, 4315–4332.
Jenner, F.E., Bennett, V.C., Nutman, A.P., Friend, C.R.L., Norman, M.D., Yaxley, G., 2009. Evidence for subduction at 3.8 Ga: geochemistry of arc-like metabasalts from the southern edge of the Isua Supracrustal Belt. Chem. Geol. 261, 83–98.
Johnson, R.W., 1977. Distribution and major element chemistry of late Cenozoic volcanoes at the southern margin of the Bismarck Sea, Papua New Guinea. Australian Bureau of Mineral Resources Report, p. 188.
Kelley, K.A., Cottrell, E., 2009. Water and the oxidation state of subduction zone magmas. Science 325, 605–607.
Kelley, K.A., Plank, T., Grove, T.L., Stolper, E.M., Newman, S., Hauri, E., 2006. Mantle melting as a function of water content beneath back-arc basins. J. Geophys. Res. 111, B09208. doi:10.1029/2005JB003732.
Klein, E.M., Langmuir, C.H., 1987. Global correlations of ocean ridge basalt chemistry with axial depth and crustal thickness. J. Geophys. Res. 92B, 8089–8115.
Komiya, T., Maruyama, S., Masuda, T., Nohda, S., Hayashi, M., Okamoto, K., 1999. Plate tectonics at 3.8–3.7 Ga: field evidence from the Isua accretionary complex, southern West Greenland. J. Geol. 107, 515–554.
Kuno, H., 1959. Geology and petrology of O-shima volcano. Int. Geol. Rev. 1, 48–59.
Lee, C.-T.A., Leeman, W.P., Canil, D., Li, Z.-X.A., 2005. Similar V/Sc systematics in MORB and arc basalts: implications for the oxygen fugacities of their mantle source regions. J. Petrol. 46, 2313–2336.
Li, Z.-X.A., Lee, C.-T.A., 2004. The constancy of upper mantle fO_2 through time inferred from V/Sc ratios in basalts. Earth Planet. Sci. Lett. 228, 483–493.
Malinovsky, D., Stenberg, A., Roduschkin, I., Andren, H., Ingri, J., Ohlander, N., Baxter, D.C., 2003. Performance of high resolution MC-ICP-MS for Fe isotope ratio measurements in sedimentary geological materials. J. Anal. At. Spectrom. 18, 687–695.
Mann, P., Taira, A., 2004. Global tectonic significance of the Solomon Islands and Ontong Java Plateau convergent zone. Tectonophysics 389, 137–190.
Martin, A.J.P., Synge, R.L.M., 1941. A new form of chromatography employing two liquid phases. 1. A theory of chromatography. 2. Application to the micro-determination of the higher monoamino-acids in proteins. Biochem. J. 35, 1358–1368.
Maruyama, S., Masuda, T., Nohda, S., Appel, P., Otofuji, Y., Miki, M., Shibata, T., Hagiya, H., 1992. The 3.9–3.8 Ga plate tectonics on the Earth: evidence from Isua, Greenland. Paper presented at the Evolving Earth Symposium. Tokyo Institute of Technology, Okazaki, Japan.
Melson, W.G., Jarosewich, E., Lundquist, C.A., 1970. Volcanic eruption at Metis Shoal, Tonga, 1967–1968: description and petrology. Smithsonian Contributions to the Earth Sciences 4 18 pp.
Métrich, N., Susini, J., Foy, E., Farges, F., Massare, D., Sylla, L., Lequien, S., Bonnin-Mosbah, M., 2006. Redox state of iron in peralkaline rhyolitic glass/melt: X-ray absorption micro-spectroscopy experiments at high temperature. Chem. Geol. 231, 350–363.
Morris, J.D., Leeman, W.P., Tera, F., 1990. The subducted component in island arc lavas: constraints from Be isotopes and B–Be systematics. Nature 344, 31–36.
Myers, J.S., 2001. Protoliths of the 3.8–3.7 Ga Isua Greenstone belt, West Greenland. Precambrian Res. 105, 129–141.
Mysen, B.O., 2006. The structural behavior of ferric and ferrous iron in aluminosilicate glass near meta-aluminosilicate joins. Geochim. Cosmochim. Acta 70, 2337–2353.
Nutman, A.P., Friend, C.R.L., 2009. New 1:20,000 scale geological maps, synthesis and history of investigation of the Isua supracrustal belt and adjacent orthogneisses, southern West Greenland: a glimpse of Eoarchaean crust formation and orogeny. Precambrian Res. 172, 189–211.
Nutman, A.P., McGregor, V.R., Friend, C.R.L., Bennett, V.C., Kinny, P.D., 1996. The Itsaq Gneiss Complex of southern West Greenland; the world's most extensive record of early crustal evolution (3900–3600 Ma). Precambrian Res. 78, 1–39.
Nutman, A.P., Bennett, V.C., Clark, R.L., Norman, M.D., 1999. Meta-igneous (non-gneissic) tonalites and quartz-diorites from an extensive ca. 3800 Ma terrain south of the Isua supracrustal belt, southern West Greenland: constraints on early crust formation. Contrib. Mineral. Petrol. 137, 364–388.
Nutman, A.P., Friend, C.R.L., Bennett, V.C., 2002a. Evidence for 3650–3600 Ma assembly of the northern end of the Itsaq Gneiss Complex, Greenland: implications for early Archaean tectonics. Tectonics 21. doi:10.1029/2000TC001203.
Nutman, A.P., McGregor, V.R., Shiraishi, K., Friend, C.R.L., Bennett, V.C., Kinny, P.D., 2002b. >3850 Ma BIF and mafic inclusions in the early Archaean Itsaq Gneiss Complex around Akilia, southern West Greenland? The difficulties of precise dating of zircon-free protoliths in migmatites. Precambrian Res. 117, 185–224.
Nutman, A.P., Bennett, V.C., Friend, C.R.L., Horie, K., Hidaka, H., 2007. 3, 850 Ma tonalites in the Nuuk region, Greenland: geochemistry and their reworking within an Eoarchean gneiss complex. Contrib. Mineral. Petrol. 154, 385–408.
Nutman, A.P., Bennett, V.C., Friend, C.R.L., Jenner, F., Wan, Y., Liu, D-Y., 2009. Eoarchaean crustal growth in West Greenland (Itsaq Gneiss Complex) and in northeastern China (Anshan area): review and synthesis. Geological Society, London, Special Publications 318, 127–154.
Ohnenstetter, D., Brown, W.L., 1992. Overgrowth textures, disequilibrium zoning, and cooling history of a glassy four-pyroxene boninite dyke from New Caledonia. J. Petrol. 33, 231–271.
Ohnenstetter, D., Brown, W.L., 1996. Compositional variation and primary water contents of differentiated interstitial and included glasses in boninites. Contrib. Mineral. Petrol. 123, 117–137.
Parkinson, I.J., Arculus, R.J., 1999. The redox state of subduction zones: insights from arc-peridotites. Chem. Geol. 160, 409–423.
Petterson, M.G., Babbs, T., Neal, C.R., Mahoney, J.J., Saunders, A.D., Duncan, R.A., Tolia, D., Magu, R., Qopoto, C., Mahoa, H., Natogga, D., 1999. Geological-tectonic framework of Solomon Islands, SW Pacific: crustal accretion and growth within an intra-oceanic setting. Tectonophysics 301, 35–60.
Poitrasson, F., 2007. Does planetary differentiation really fractionate iron isotopes? Earth Planet. Sci. Lett. 256, 484–492.
Poitrasson, F., Freydier, R., 2005. Heavy iron isotope composition of granites determined by high resolution MC-ICP-MS. Chem. Geol. 222, 132–147.
Poitrasson, F., Halliday, A.N., Lee, D.-C., Levasseur, S., Teutsch, N., 2004. Iron isotope differences between Earth, Moon, Mars and Vesta as possible records of contrasted accretion mechanisms. Earth Planet. Sci. Lett. 223, 253–266.

Poitrasson, F., Levasseur, S., Teutsch, N., 2005. Significance of iron isotope mineral fractionation in pallasites and iron meteorites for the core–mantle differentiation of terrestrial planets. Earth Planet. Sci. Lett. 234, 151–164.
Polat, A., Hofmann, A.W., 2003. Alteration and geochemical patterns in the 3.7–3.8 Ga Isua greenstone belt, West Greenland. Precambrian Res. 126, 197–218.
Polat, A., Hofmann, A.W., Rosing, M.T., 2002. Boninite-like volcanic rocks in the 3.7–3.8 Ga Isua greenstone belt, West Greenland: geochemical evidence for intra-oceanic subduction zone processes in the early Earth. Chem. Geol. 184, 231–254.
Polyakov, V.B., 2009. Equilibrium iron isotope fractionation at core–mantle boundary conditions. Science 323, 912–914.
Polyakov, V.B., Mineev, S.D., 2000. The use of Mössbauer spectroscopy in stable isotope geochemistry. Geochim. Cosmochim. Acta 64, 849–865.
Polyakov, V.B., Clayton, R.N., Horita, J., Mineev, S.D., 2007. Equilibrium iron isotope fractionation factors of minerals: reevaluation from the data of nuclear inelastic resonant X-ray scattering and Mössbauer spectroscopy. Geochim. Cosmochim. Acta 71, 3833–3846.
Rollinson, H., 2007. Recognising early Archaean mantle: a reappraisal. Contrib. Mineral. Petrol. 154, 241–252.
Rosing, M.T., Rose, N.M., Bridgwater, D., Thomsen, H.S., 1996. Earliest part of Earth's stratigraphic record: a reappraisal of the >3.7 Ga Isua (Greenland) supracrustal sequence. Geology 24, 43–46.
Rubin, A.E., 1984. The Blithfield meteorite and the origin of sulfide-rich, metal-poor clasts and inclusions in brecciated enstatite chondrites. Earth Planet. Sci. Lett. 67, 273–283.
Schauble, E.A., 2004. Applying stable isotope fractionation theory to new systems. Rev. Mineral. Geochem. 55, 65–111.
Schmidt, R.G., 1957. Geology of Saipan, Mariana Islands: petrology of the volcanic rocks. Geological Survey Professional Paper 280-B-D, pp. 127–174.
Schoenberg, R., von Blanckenburg, F., 2005. An assessment of the accuracy of stable Fe isotope ratio measurements on samples with organic and inorganic matrices by high-resolution multicollector ICP-MS. Int. J. Mass Spectrom. 242, 257–272.
Schoenberg, R., von Blanckenburg, F., 2006. Modes of planetary-scale Fe isotope fractionation. Earth Planet. Sci. Lett. 252, 342–359.
Schoenberg, R., Marks, M.A.W., Schuessler, J.A., von Blanckenburg, F., Markl, G., 2009. Fe isotope systematics of coexisting amphibole and pyroxene in the alkaline igneous rock suite of the Illímaussaq Complex, South Greenland. Chem. Geol. 258, 65–77.
Schuessler, J.A., Schoenberg, R., Behrens, H., von Blanckenburg, F., 2007. The experimental calibration of the iron isotope fractionation factor between pyrrhotite and peralkaline rhyolitic melt. Geochim. Cosmochim. Acta 71, 417–433.
Schuessler, J.A., Schoenberg, R., Sigmarsson, O., 2009. Iron and lithium isotope systematics of the Hekla volcano, Iceland—evidence for Fe isotope fractionation during magma differentiation. Chem. Geol. 258, 78–91.
Sears, D.W.G., Dodd, R.T., 1988. 1.1 Overview and classification of meteorites. In: Kerridge, J.F., Matthews, M.S. (Eds.), Meyeorites and the Early Solar System. University of Arizona Press, Tucson, pp. 3–31.
Shahar, A., Young, E.D., Manning, C.E., 2008. Equilibrium high-temperature Fe isotope fractionation between fayalite and magnetite: an experimental approach. Earth Planet. Sci. Lett. 268, 330–338.
Shiraki, K., Kuroda, N., Urano, H., Maruyama, S., 1980. Clinoenstatite in boninites from the Bonin Islands, Japan. Nature 285, 31–32.
Stern, R.J., Fouch, M.J., Klemperer, S.L., 2003. An overview of the Izu–Bonin–Mariana subduction factory. In: Eiler, J., Hirschmann, M. (Eds.), Inside the Subduction Factory: American Geophysical Union Geophysical Monograph, vol. 138, pp. 175–222.
Stolper, E., Newman, S., 1994. The role of water in the petrogenesis of Mariana trough magmas. Earth Planet. Sci. Lett. 121, 293–325.
Strelow, F.W.E., 1980. Improved separation of iron from copper and other elements by anion-exchange chromatography on a 4% cross-linked resin with high concentration of hydrochloric acid. Talanta 27, 727–732.
Tang, H., Dauphas, N., Craddock, P.R., 2009. High precision iron isotopic analyzes of meteorites and terrestrial rocks: ^{6}Fe distribution and mass fractionation laws. LPSC 40, #1903.
Tatsumoto, M., Knight, R.J., 1969. Isotopic composition of lead in volcanic rocks from central Honshu—with regards to basalt genesis. Geochem. J. 3, 53–86.
Taylor, P.D.P., Maeck, R., De Bièvre, P., 1992. Determination of the absolute isotopic composition and atomic weight of a reference sample of natural iron. Int. J. Mass Spectrom. 121, 111–125.
Teng, F.-Z., Dauphas, N., Helz, R.T., 2008. Iron isotope fractionation during magmatic differentiation in Kilauea Iki lava lake. Science 320, 1620–1622.
Wadhwa, M., 2001. Redox state of Mars upper mantle and crust from Eu anomalies in shergottite pyroxenes. Science 291, 1527–1530.
Wadhwa, M., 2008. Redox conditions on small bodies, the Moon and Mars. Rev. Mineral. Geochem. 68, 493–510.
Weyer, S., Ionov, D.A., 2007. Partial melting and melt percolation in the mantle: the message from Fe isotopes. Earth Planet. Sci. Lett. 259, 119–133.
Weyer, S., Schwieters, J.B., 2003. High precision Fe isotope measurements with high mass resolution MC-ICPMS. Int. J. Mass Spectrom. 226, 355–368.
Weyer, S., Anbar, A.D., Brey, G.P., Münker, C., Mezger, K., Woodland, A.B., 2005. Iron isotope fractionation during planetary differentiation. Earth Planet. Sci. Lett. 240, 251–264.
Weyer, S., Anbar, A.D., Brey, G.P., Münker, C., Mezger, K., Woodland, A.B., 2007. Fe-isotope fractionation during partial melting on Earth and the current view on the Fe-isotope budgets of the planets (reply to the comments of F. Poitrasson and to the comments of B.L. Beard and C.M. Johnson). Earth Planet. Sci. Lett. 256, 638–646.
Wilke, M., Partzsch, G.M., Bernhardt, R., Lattard, D., 2005. Determination of the iron oxidation state in basaltic glasses using XANES at the K-edge. Chem. Geol. 220, 143–161.
Williams, H.M., Peslier, A.H., McCammon, C., Halliday, A.N., Levasseur, S., Teutsch, N., Burg, J.-P., 2005. Systematic iron isotope variations in mantle rocks and minerals: the effects of partial melting and oxygen fugacity. Earth Planet. Sci. Lett. 235, 435–452.
Williams, H.M., Nielsen, S.G., Renac, C., Griffin, W.L., O'Reilly, S.Y., McCammon, C.A., Pearson, N., Viljoen, F., Alt, J.C., Halliday, A.N., 2009. Fractionation of oxygen and iron isotopes by partial melting processes: implications for the interpretation of stable isotope signatures in mafic rocks. Earth Planet. Sci. Lett. 283, 156–166.
Woodhead, J.D., Johnson, R.W., 1993. Isotopic and trace element profiles across the New Britain island arc, Papua New Guinea. Contrib. Mineral. Petrol. 113, 479–491.
Woodhead, J.D., Eggins, S.M., Johnson, R.W., 1998. Magma genesis in the New Britain Island Arc: further insights into melting and mass transfer processes. J. Petrol. 39, 1641–1668.
Woodhead, J.D., Hergt, J.M., Davidson, J.P., Eggins, S.M., 2001. Hafnium isotope evidence for 'conservative' element mobility during subduction zone processes. Earth Planet. Sci. Lett. 192, 331–346.
Woodland, A.B., Kornprobst, J., Tabit, A., 2006. Ferric iron in orogenic lherzolite massifs and controls of oxygen fugacity in the upper mantle. Lithos 89, 222–241.